Distinct spermiogenic phenotypes underlie sperm elimination in the *Segregation Distorter* meiotic drive system

Marion Herbette[1], Xiaolu Wei[2], Ching-Ho Chang[3,4], Amanda M. Larracuente[4], Benjamin Loppin[1] and Raphaëlle Dubruille[1*]

* corresponding author: raphaelle.renard-dubruille@ens-lyon.fr

Author affiliations

1. Laboratoire de Biologie et Modélisation de la Cellule, CNRS UMR 5239, École Normale Supérieure de Lyon, University of Lyon, France

2. University of Rochester Medical Center, Department of Biomedical Genetics, Rochester, NY USA

3. Present address: Fred Hutchison Cancer Research Center, Seattle, WA, USA

4. University of Rochester Department of Biology, Rochester, NY, USA

ORCID MH 0000-0002-7683-3207
ORCID XW 0000-0001-9952-3757
ORCID CHC 0000-0001-9361-1190
ORCID AML 0000-0001-5944-5686
ORCID BL 0000-0002-7166-9233
ORCID RD 0000-0002-7710-3716

Running title: Sperm elimination in *Segregation Distorter*

Keywords: *Segregation Distorter*, meiotic drive, spermiogenesis, histone-to-protamine transition, satellite DNA, *Drosophila melanogaster*

Abstract

Segregation Distorter (*SD*) is a male meiotic drive system in *Drosophila melanogaster.* Males heterozygous for a selfish *SD* chromosome rarely transmit the homologous SD^+ chromosome. It is well established that distortion results from an interaction between *Sd*, the primary distorting locus on the *SD* chromosome and its target, a satellite DNA called *Rsp,* on the SD^+ chromosome. However, the molecular and cellular mechanisms leading to post-meiotic SD^+ sperm elimination remain unclear. Here we show that SD/SD^+ males of different genotypes but with similarly strong degrees of distortion have distinct spermiogenic phenotypes. In some genotypes, SD^+ spermatids fail to fully incorporate protamines after the removal of histones, and degenerate during the individualization stage of spermiogenesis. In contrast, in other SD/SD^+ genotypes, protamine incorporation appears less disturbed, yet spermatid nuclei are abnormally compacted, and mature sperm nuclei are eventually released in the seminal vesicle. Our analyses of different SD^+ chromosomes suggest that the severity of the spermiogenic defects associates with the copy number of the *Rsp* satellite. We propose that when *Rsp* copy number is very high (> 2000), spermatid nuclear compaction defects reach a threshold that triggers a checkpoint controlling sperm chromatin quality to eliminate abnormal spermatids during individualization.

Introduction

In sexually reproducing organisms, the production of haploid gametes from diploid germ cells ensures that two alleles of the same locus are equally transmitted to the progeny. However, selfish genetic elements recurrently emerge in genomes and manipulate gametogenesis in either sex to promote their own transmission thus resulting in the distortion of Mendelian ratios (Lindholm *et al.,* 2016). Although "meiotic drivers" are widespread across plants, animals and fungi, male-specific meiotic drive systems are particularly well studied in *Drosophila* species, where 19 independent distorters are currently known (Lindholm *et al.,* 2016; Courret *et al.,* 2019). While most of these drive systems are sex-linked and thus distort sex ratios, one of the most famous male-specific meiotic drivers is an autosomal selfish gene complex called *Segregation Distorter* (*SD*) in *D. melanogaster* (Sandler *et al.,* 1959, Larracuente and Presgraves, 2012).

Based on the cytological phenotype they cause, male-specific meiotic drive systems can be classified into two types: those that induce meiotic defects, such as the *Paris* sex ratio system from *D. simulans*, and those that result in post-meiotic defects—and are thus called meiotic drive systems in a broad sense (Courret *et al.,* 2019). *SD* is by far the best studied and documented system and belongs to the second category. It was first described in 1959 after the discovery of second chromosomes (called *SD* chromosomes) that induced distortion of the expected Mendelian ratio (Sandler *et al.,* 1959): in the appropriate genetic background, heterozygous SD/SD^{+} males transmit the *SD* chromosome to 95-100% of their progenies.

While *SD* systems are selfish gene complexes consisting of multiple factors that contribute to drive, two main components are molecularly characterized: *Sd,* the primary driver shared by all *SD* chromosomes, and *Responder (Rsp),* its genetic target on SD^{+} chromosome (Figure 1A). *Sd* is an incomplete duplication of the *RanGAP* gene (hereafter called *Sd-RanGAP*), that encodes a C-terminus truncated version of the Ran GTPase Activating Protein (RanGAP) (Powers and Ganetzky,

1991; Merrill *et al.,* 1999; Larracuente and Presgraves, 2012). RanGAP is a cytosolic GTPase-activating enzyme that binds to nuclear pores and hydrolyzes Ran-GTP into Ran-GDP, which aids in the transport of proteins and some RNAs from the cytosol to the nucleus (Steggerda and Paschal, 2002). The truncated Sd-RanGAP protein is still enzymatically active but mislocalizes in primary spermatocytes, the diploid cells that will give rise to spermatids after meiosis (Kusano *et al.,* 2001). *Responder* (*Rsp*) is a satellite DNA (hereafter satDNA) that consists of dimers of two related ~120-bp AT-rich sequences that are tandemly repeated in the pericentromeric heterochromatin on the right arm of the second chromosome (Wu *et al.,* 1988; Pimpinelli and Dimitri, 1989) (Figure 1A). The number of 120-bp *Rsp* monomers varies in natural populations and positively correlates with their sensitivity to distortion (Wu *et al.,* 1988; Pimpinelli and Dimitri, 1989; Lyttle, 1991; Larracuente and Presgraves, 2012). Indeed, SD^+ chromosomes with high *Rsp* copy number (e.g. >2000) are super sensitive (Rsp^{ss}) to drive and are rarely transmitted to the progeny in SD/SD^+ males. However, SD^+ chromosomes with intermediate *Rsp* copy number (*e.g.* 700-1000) show a continuous range of drive sensitivity (Rsp^s) and SD^+ chromosomes with low *Rsp* copy number (*e.g.* <200) are insensitive to drive (Rsp^i). *SD* chromosomes have Rsp^i alleles with very low *Rsp* copy number (< 20) and are thus insensitive to their own drive (Wu *et al.,* 1988; Pimpinelli and Dimitri, 1989; Lyttle 1991; Larracuente and Presgraves, 2012).

While identifying these key genetic elements was a major step forward in understanding the molecular principles of *SD*, the mechanisms by which these elements genetically interact and eventually lead to the specific elimination of SD^+ Rsp^s gametes remain mysterious. The first obvious defects appear during spermiogenesis, the maturation of the haploid spermatids into mature sperm cells. By transmission electron microscopy, Tokuyasu and colleagues showed that about half of spermatids—supposedly the ones containing the SD^+ chromosome—have abnormally decompacted chromatin compared to their sister spermatid nuclei (Tokuyasu *et al.,* 1977). Importantly, spermiogenesis is characterized by a dramatic reorganization of spermatid nuclei which reduce in

volume and adopt a characteristic needle-shape (Fabian and Brill, 2012; see Figure 1B for a description of *Drosophila* spermatogenesis). This extreme nuclear compaction is primary driven by a global chromatin-remodeling process known as the histone-to-protamine transition, whereby most of the histones are eliminated and replaced by Sperm Nuclear Basic Proteins (SNBPs), such as the archetypal protamines in mammals (Lewis, 2003). In *Drosophila*, nearly all histones are eliminated at the onset of the transition and are replaced by transition proteins, such as Tpl94D (Rathke *et al.,* 2007). Then, transition proteins are also eliminated and at least four protamine-like SNBPs of the MST-HMG Box family are incorporated: Mst35Ba/b (ProtA/B), Prtl99C and Mst77F (Jayaramaiah Raja and Renkawitz-Pohl, 2005; Rathke *et al.,* 2014; Eren-Ghiani *et al*., 2015; Doyen *et al.,* 2015). Interestingly, in 1982, Hauschteck-Jungen and Hartl showed that half of the spermatids in SD/SD^+ males stained weakly with a fluorescent dye that detects basic proteins (Hauschteck-Jungen and Hartl, 1982). The authors thus proposed that the histone-to-protamine transition—that had not yet been characterized in *Drosophila* at that time—failed to occur in the SD^+ nuclei. However, other studies suggested that SD^+ spermatids differentiated into spermatozoa and were transferred to females, but did not fertilize eggs (Peacock and Erickson, 1965; Tokuyasu *et al.,* 1977). It is still unclear if the elimination of sperm cells in SD/SD^+ males results from a failure in SNBP deposition in SD^+ spermatids, and more generally, what cytological events lead to SD^+ sperm elimination in the *SD* system.

Here we studied the histone-to-protamine transition in different strong *SD* genotypes with similar levels of segregation distortion. We show that the cytological phenotypes of *SD* males are variable, even though they share strong distortion strength, and this variability is largely associated with the number of *Rsp* repeats. Moreover, we show that the cytological phenotype can be profoundly modified by a genetic suppressor on the X chromosome.

Results

In *SD* males, nuclear defects are observed during the histone-to-protamine transition

To determine when *Rsp*^{s} gametes were eliminated in *SD/SD*$^+$ males, we chose to study spermatogenesis in two different genetic backgrounds that confer high distortion levels (see Table 1 for *k* values, which are the ratio of flies carrying the *SD* chromosome over the total progeny of tested males). We used the *SD*$^+$ *cn*^{1} *bw*^{1} chromosome, a classical *Rsp*^{s} chromosome, that we combined with the *SD-Mad* distorter chromosome, a strong classical distorter chromosome isolated from a wild population in Madison, WI (Brittnacher and Ganetzky, 1983). We also used the *SD*$^+$ *Rsp*^{s} dominantly marked balancer chromosome, *In(2LR)Gla* (hereafter *Gla*, Presgraves *et al.,* 2009) that we combined with the *SD5* distorter chromosome (Brittnacher and Ganetzky, 1983), another classical strong *SD* chromosome. To visualize the histone-to-protamine transition, we introduced a *protB-GFP* transgene—that expressed the *Drosophila* SNBP Protamine B (or Mst35Bb) fused to GFP—in the *SD* backgrounds. Both *Gla/SD5; protB-GFP* and *cn*^{1} *bw*^{1}*/SD-Mad; protB-GFP* males (hereafter *Gla/SD5* and *cn*^{1} *bw*^{1}*/SD-Mad)* harbored very strong distortion levels (*k* values 1 and 0.998, respectively, Table 1).

In *Drosophila*, spermatogenesis starts at the tip of the tubular testis and progresses along the axis. Germ stem cells divide asymmetrically to produce another germ stem cell and a spermatogonium. The spermatogonium goes through 4 incomplete mitoses (without cytokinesis) and forms a cyst of 16 spermatocytes interconnected by cytoplasmic bridges. These spermatocytes then undergo meiosis and give rise to cysts of 64 haploid spermatids. Each cyst of 64 spermatids then differentiates into mature sperm cells in synchrony during spermiogenesis (Fuller, 1993; Figure 1B). We first observed the general organization of spermatogenesis in *SD/SD*$^+$ male testes. In both *SD* backgrounds, spermatogenesis appeared normal until the histone-to-protamine transition, as previously reported (Peacock and Erickson, 1965; Figure 1C and Figure S1). During the histone-to-protamine incorporation, we observed many cysts containing both elongated spermatid nuclei and

abnormally-shaped nuclei, often lagging behind. The abnormally-shaped nuclei also have loosely packed spermatid bundles indicating that they were eliminated before the end of spermiogenesis (Figure 1D and Figure S1). The abnormally shaped nuclei varied in appearance: some nuclei lost their elongated shape and were roundish, while some others were curled or crumpled. DNA-FISH analyses of *Gla/SD5* testes confirmed that the abnormally-shaped spermatid nuclei inherited the SD^+ chromosome with a large *Rsp* satDNA block and were eliminated (Figure 1E). However, we noticed that the phenotype of cn^1 bw^1*/SD-Mad* males was more variable. In fact, although the histone-to-protamine transition was perturbed, we observed the presence of some cysts with a less severe phenotype (Figure S1). Moreover, the DNA-FISH *Rsp* probe stained both abnormally-shaped spermatid nuclei and few nuclei with an apparent normal shape (Figure 1E). These observations suggested that the mode of spermatid elimination may differ between cn^1 bw^1*/SD-Mad* and *Gla/SD5* genotypes.

Histone elimination and Tpl94D transient incorporation are slightly delayed in *Gla/SD5* males

To determine the precise stage of SD^+ spermatid nuclei elimination and the defects that these nuclei may have, we analyzed the histone-to-protamine transition in *SD* males in detail. We first stained testes for histones and the transition protein Tpl94D. In cn^1 bw^1*/SD-Mad* testes, the dynamics of histone elimination and transient Tpl94D expression were comparable to control *Gla/CyO* males (Figure 2). Histone signals progressively decreased as Tpl94D signal increased in elongating spermatids. Then, the Tpl94D signal also vanished and at the end of spermiogenesis, histones and Tpl94D were undetectable in all nuclei. In *Gla/SD5* males, we also observed progressive histone elimination, transient expression of Tpl94D, and the eliminated spermatid nuclei were all negative for histones and Tpl94D. However, we repeatedly observed some spermatid nuclei (ca. 4-8 per cyst) with a faint histone signal in cysts that were also positive for Tpl94D (Figure 2, white arrows and

see oversaturated image). At this stage, histones were barely detected in control and *cn*^{1} *bw*^{1}*/SD-Mad* flies (Figure 2). We also observed that about half of the nuclei showed a weaker Tpl94D signal than the other half (Figure 2). These observations suggested that histone elimination and transient Tpl94D expression were delayed in *SD*$^{+}$ spermatid nuclei in *Gla/SD5* males but not in *cn*^{1} *bw*^{1}*/SD-Mad* males.

Protamine incorporation is incomplete in *SD*$^{+}$ nuclei of *Gla/SD5* males and stops prematurely

We then studied progression of protamine incorporation in *Gla/SD5* and *cn*^{1} *bw*^{1}*/SD-Mad* testes using the *protB-GFP* transgene. To determine more precisely the stage of spermatid differentiation, we stained testes for F-actin to reveal individualization complexes (IC). IC are actin cones that form around spermatid nuclei at the end of the histone-to-protamine transition and mark the onset of individualization. During this process, IC move along spermatid axes to remove excess materials and cytoplasm and invest each of the 64 interconnected spermatids with their own cell membrane (Figure 3A; Fabian and Brill, 2012; Steinhauer, 2015).

In *Gla/SD5* testes, all nuclei in cysts of early elongating spermatids were normally shaped and had started to incorporate protamines. However, about half of the nuclei showed weaker ProtB-GFP signals compared to the other half (pre-IC, Figure 3B and Figure 3C). Then, when individualization started, the weakly stained nuclei in *Gla/SD5* appeared larger than their sister nuclei (IC, Figure 3B). At the end of spermiogenesis, the *SD*$^{+}$ nuclei were abnormally shaped, weakly stained with ProtB-GFP and lagged behind the rest of the bright ProtB-GFP positive, needle-shaped nuclei (post-IC, Figure3B). This suggested that in *Gla/SD5* males, *SD*$^{+}$ spermatid nuclei incorporated fewer SNBPs and were eliminated during individualization. This phenotype was comparatively weaker and more variable in *cn*^{1} *bw*^{1}*/SD-Mad* testes. In each cyst, we observed weakly stained ProtB-GFP (pre-IC) and abnormally shaped spermatid nuclei (IC and post-IC) but

they were infrequent and varied in number (Figure 3B). These observations suggested that in *cn*^{1} *bw*^{1}*/SD-Mad*, the histone-to-protamine transition was generally less disturbed in *SD*$^{+}$ nuclei and a significant fraction of these nuclei progressed normally through this important chromatin transition.

Chromatin compaction is abnormal in *SD*$^{+}$ spermatids in *SD/SD*$^{+}$ males

Previous electron microscopy studies reported that half of nuclei presented chromatin condensation defects within the same cyst of elongating spermatids from *SD/SD*$^{+}$ males (Tokuyasu *et al.,* 1977). We thus examined chromatin compaction using an antibody that recognizes double-stranded DNA (anti-dsDNA) to take advantage of the reduced accessibility to spermatid DNA after chromatin compaction. Indeed, in sperm heads, chromatin is so tightly compacted that nuclei are refractory to antibody staining (Bonnefoy *et al.,* 2007). As expected, in wildtype testes, the anti-dsDNA antibody stained somatic and germinal nuclei except IC and post-IC stage spermatids and sperm nuclei (Figure S2). Moreover, the staining strength was directly and negatively linked to the level of chromatin compaction. We then stained control and *SD*/*SD*$^{+}$ testes with the anti-dsDNA antibody. In control *Gla/CyO* males, all spermatid nuclei in pre-IC cysts were evenly stained with the anti-dsDNA antibody. As protamine incorporation and chromatin compaction progressed, this staining vanished (Figure 4). In contrast, in *Gla/SD5* testes, the anti-dsDNA staining appeared stronger in about half of the spermatid nuclei in pre-IC cysts (Figure 4). These nuclei corresponded to the ones that were weakly stained with ProtB-GFP, supporting the hypothesis that *SD*$^{+}$ nuclei failed to fully incorporate SNBPs and compact their chromatin properly. Moreover, at later stages (IC and post-IC; Figure 4), the eliminated nuclei were brightly stained with the anti-dsDNA antibody, whereas the nuclei that differentiated normally were all negative for this marker. In *cn*^{1} *bw*^{1}/*SD-Mad* testes, this phenotype was again weaker and highly variable. Notably, in IC and post-IC cysts, abnormally-shaped spermatid nuclei brightly stained with the anti-dsDNA antibody were

less frequent. However, we also observed needle-shaped nuclei weakly stained with the anti-dsDNA antibody that were included in the bundles of individualized spermatids (Figure 4).

Seminal vesicles of *cn*^{1} *bw*^{1}/*SD-Mad* males contain abnormally condensed sperm nuclei

Our previous observations of *cn*^{1} *bw*^{1}/*SD-Mad* testes suggested that abnormally compacted *SD*$^+$ nuclei escaped elimination during individualization and differentiated into mature spermatozoa. To test this hypothesis, we examined seminal vesicle contents stained with the anti-dsDNA antibody. As expected, in *cn*^{1} *bw*^{1}/*CyO* and *Gla/CyO* control males, seminal vesicles were filled with needle-shaped sperm nuclei brightly stained with ProtB-GFP that were almost all negative for the anti-dsDNA antibody (Figure 5A and Figure S3). In *Gla/SD5* males, seminal vesicles were smaller and contained fewer nuclei than control seminal vesicles. In all seminal vesicles, nearly all sperm nuclei were needle-shaped, brightly stained with ProtB-GFP and negative for the anti-dsDNA antibody. In striking contrast, *cn*^{1} *bw*^{1}/*SD-Mad* seminal vesicles contained many anti-dsDNA positive sperm nuclei (Figure 5A). Some of these nuclei were abnormally shaped but most of them were needle shaped, suggesting that although the *SD*$^+$ nuclei acquired an elongated shape, their chromatin was not properly compacted. To verify that these nuclei corresponded to *SD*$^+$ *Rsp*^{s} nuclei, we performed DNA-FISH on squashed seminal vesicles with a *Rsp* probe and a control probe specific to the *359 bp* satDNA, a large X-linked satDNA block (Figure 5B). In *Gla/SD5* male vesicles, about half of nuclei were stained with the *359 bp* probe as expected, while *Rsp* positive nuclei were very rare or absent, confirming that nearly all *SD*$^+$ *Rsp*^{s} spermatids were eliminated during spermiogenesis. On the contrary, in *cn*^{1} *bw*^{1}/*SD-Mad* males, many sperm nuclei were stained with the *Rsp* probe, confirming that *SD*$^+$ *Rsp*^{s} nuclei were released in the seminal vesicle. Importantly, since the *cn*^{1} *bw*^{1}/*SD-Mad* males exhibited very high levels of segregation distortion (*k* value 0.998; Table 1), we inferred that these abnormally condensed sperm cells were unable to fertilize eggs, as suggested by Peacock and Erickson (1965).

Image analysis and quantification revealed that seminal vesicles contained about 30% and 2% of anti-dsDNA positive sperm nuclei in *cn*^{1} *bw*^{1}*/SD-Mad* and *Gla/SD5* males, respectively (for each one, n=5, where n is the number of analyzed seminal vesicles, Figure 5C). This quantification showed that in *Gla/SD5* males, less than one *SD*$^{+}$ nucleus of 32 *SD*$^{+}$ expected nuclei per cyst on average was released in the seminal vesicle, whereas, in *cn*^{1} *bw*^{1}*/SD-Mad* males, 13.8 of 32 *SD*$^{+}$ nuclei per cyst on average were released. From our previous observation, we suspected that the number of eliminated nuclei was variable from one cyst to another in *cn*^{1} *bw*^{1}*/SD-Mad* males. In support of this observation, Tokuyasu and colleagues reported that in *cn*^{1} *bw*^{1}*/ SD72* males, the number of abnormal spermatids that failed to individualize in a cyst varied from 0 to 32 but that the number of spermatids with incompletely condensed chromatin was nearly 32 (Tokuyasu *et al.,* 1972). Taken together, our results showed that the cytological phenotypes of two *SD/SD*$^{+}$ male genotypes with very high and comparable distortion levels were largely different. In *Gla/SD5* males, *SD*$^{+}$ spermatids are systematically eliminated during individualization whereas, in *cn*^{1} *bw*^{1}*/SD-Mad* males, *SD*$^{+}$ abnormal sperm cells are released in the seminal vesicle.

We then wondered whether this difference was linked to the *SD*$^{+}$ *Rsp*^{s} or the *SD* chromosome. We thus set up reciprocal crosses to generate *cn*^{1} *bw*^{1}*/SD5* and *Gla/SD-Mad* males and used DNA-FISH and the anti-dsDNA antibody to detect *SD*$^{+}$ *Rsp*^{s} sperm nuclei in seminal vesicles. While we observed many *SD*$^{+}$ *Rsp*^{s} escaper nuclei in the seminal vesicles of *cn*^{1} *bw*^{1}*/SD5* males, we seldom detected *SD*$^{+}$ *Rsp*^{s} nuclei in *Gla/SD-Mad* seminal vesicles (Figure 5A and 5C). Moreover, during the histone-to-protamine transition, half of spermatid nuclei in *Gla/SD-Mad* incorporated fewer protamines, were abnormally compacted and eliminated during individualization, similar to what we observed in *Gla/SD5* males (Figure S4). On the contrary, in *cn*^{1} *bw*^{1}*/SD5* testes, this phenotype was weaker and variable, as we previously observed in *cn*^{1} *bw*^{1}*/SD-Mad* (Figure S4). These results thus support the hypothesis that the difference between the two *SD* cytological phenotypes depends on the *SD*$^{+}$ *Rsp*^{s} chromosome.

Systematic *SD*$^+$ spermatid elimination during individualization occurs when *Rsp* carry 2000 copies or more

Since the strength of *SD* male segregation distortion positively correlates with *Rsp* copy number (Wu *et al.,* 1988; Pimpinelli and Dimitri, 1989), we wondered whether this factor could account for the observed difference between cytological phenotypes. The structure of the *Rsp* satDNA locus on the *cn*^{1} *bw*^{1} chromosome carried by the *iso-1* strain has been characterized in detail with single-molecule sequencing long reads and validated with molecular and computational approaches (Khost *et al.,* 2017). The major *Rsp* locus of *iso-1* flies contained ≈1050 *Rsp* repeats spread across ≈170 kb. However, the copy number and the organization of the *Rsp* satDNA of the *Gla* chromosome, is unknown. We thus estimated the number of *Rsp* satDNA copies on the *Gla* chromosome relative to *cn*^{1} *bw*^{1} chromosome by quantitative PCR on genomic DNA using two sets of primers that we designed using the published canonical *Rsp* left and right sequences (Khost *et al.,* 2017). We used *cn*^{1} *bw*^{1}*/SD-Mad* flies to normalize the quantification and validated by quantifying copy number in *SD-Mad* and *cn*^{1} *bw*^{1} homozygous flies. Our results showed that *SD-Mad*/*SD-Mad* carried about 20 copies consistent with previous studies (Wu *et al.,* 1988) and *cn*^{1} *bw*^{1} homozygous flies carried ≈2000 copies, as expected. Interestingly, the quantification of *Gla/SD-Mad* flies revealed that the *Gla* chromosome carried 2800-3800 copies, depending on the primer set (Figure 6A). This variation may be due to the organization of the *Rsp* satDNA on the *Gla* chromosome. Indeed, although the canonical *Rsp* repeat is a dimer of related left and right *Rsp* sequences, tandem monomeric repeats (e.g. multiple right *Rsp*) are occasionally interspersed with the dimers. Therefore, the number of left and right *Rsp* in a locus can vary. Our quantification nevertheless suggested that the *Gla* chromosome contained at least twice as many repeats as the *cn*^{1} *bw*^{1} chromosome. To verify that the *Gla* chromosome carried a larger *Rsp* satDNA block, we also performed DNA-FISH on squashed spermatid nuclei. Consistent with our expectations, *Rsp*

fluorescent signals were larger in *Gla* spermatid nuclei compared to *cn*^{1} *bw*^{1} (Figure S5). These results thus support our hypothesis that the cytological phenotype is linked to *Rsp* copy number.

To further challenge our hypothesis, we studied the phenotype of other *SD/SD*$^{+}$ males bearing the *SD-Mad* chromosome combined with *SD*$^{+}$ chromosomes carrying different *Rsp* copy numbers. We selected three strains from the Drosophila Genetics Reference Panel (DGRP)—a collection of sequenced inbred *D. melanogaster* lines derived from wild-caught flies (Mackay *et al.,* 2012; Huang *et al.,* 2014)—that carried different *Rsp* copy numbers that we estimated by qPCR: *RAL-313* (≈1000 copies), *RAL-309* (≈1300 copies) and *RAL-380* (≈2500-2700 copies) (Figure 6A). We also performed DNA-FISH on spermatid nuclei and quantified the size of *Rsp* signals relative to nuclear size. The relative size of *Rsp* signals was also higher in *RAL-380* and smaller in *RAL-313* thus corroborating the qPCR results (Figure S5). We crossed these lines to *SD-Mad; protB-GFP* flies to examine testes and seminal vesicles of the male progeny. Interestingly, the cytological phenotype of *RAL-380/SD-Mad* males was similar to *Gla/SD5*: in pre-IC cysts, about half of spermatid nuclei showed a weaker ProtB-GFP signal and stronger anti-dsDNA staining compared to the other half. In IC and post-IC cysts, these nuclei were abnormally shaped and compacted (Figure 6B). Finally, seminal vesicles contained almost no anti-dsDNA positive sperm nuclei (Figure 6B). In contrast, the distorter males that carried *SD*$^{+}$ chromosomes from the *RAL-309* and *RAL-313* strains, that contained fewer *Rsp* copies than *RAL-380*, showed a phenotype similar to *cn*^{1} *bw*^{1}/*SD* males (Figure 6B). These results confirmed that the phenotype of systematic spermatid elimination before the release in seminal vesicles is associated with a very high *Rsp* copy number. They also suggested a threshold for *Rsp* copy number (>1300) above which spermatid elimination is systematic during individualization.

A suppressor on the X modifies the phenotype of spermatid elimination

In the course of our experiments, we noticed that distortion levels were lower when we used females from the *RAL-313*, *RAL-309* and *RAL-380* strains in our crosses to produce *SD*/*SD*$^+$ males (see *k* values in Table 1 and Figure S7 for a description of the crosses). This observation suggested that the X chromosomes of these strains carried one or more genetic elements that act as a weak suppressor of *SD* (hereafter *Su(SD)X-380, Su(SD)X-309* and *Su(SD)X-313*). To study the impact of these suppressors on spermiogenesis progression, we generated *SD/SD*$^+$ males bearing *Su(SD)X* and the *protB-GFP* transgene and stained their testes with DAPI and F-actin. Strikingly, in males that carried an *SD*$^+$ chromosome with >2000 copies (*RAL-380*), the cytological phenotype was profoundly modified by the presence of *Su(SD)X-380*. Indeed, whereas seminal vesicles of w^{1118}; *RAL-380/SD-Mad* males contained <2% of anti-dsDNA positive nuclei, we counted up to ≈30% of such nuclei in *Su(SD)X-380*; *RAL-380/SD-Mad* (Figure 7). Moreover, the histone-to-protamine transition in *Su(SD)X-380*; *RAL-380/SD-Mad* males appeared less disturbed (Figure S6). It thus appeared that the presence of *Su(SD)X-380* might allow for the release of many *SD*$^+$ nuclei in the seminal vesicles. However, the strong segregation distortion (*k* value 0.941 with *Su(SD)X-380* versus 0.997 without, Table 1) suggested that most of these nuclei were not functional. In the *RAL-313* and *RAL-309 SD/SD*$^+$ males, *Su(SD)X* had no significant effect on spermiogenesis progression. However, the proportion of anti-dsDNA positive nuclei in the seminal vesicles of *Su(SD)X-313*; *RAL-313/SD-Mad* and *Su(SD)X-309*; *RAL-309/SD-Mad* males increased by ≈15 and ≈18%, respectively. These results indicated that some X-linked suppressors modified spermatid elimination efficiency at individualization. Thus, a modest effect on segregation distortion levels could underly substantial modifications of the cytological phenotype.

Discussion

Our study shows that the cytological phenotypes of strong distorter males (*k* value> 0.95) can be classified into at least two categories. In the first category, *SD*$^+$ spermatid nuclei show a delay

in the initial steps of the histone-to-protamine transition, followed by a premature arrest of protamine incorporation, abnormal nuclear condensation and systematic elimination during individualization. In the second category, SD^+ spermatid nuclei display fewer disturbances of the histone-to-protamine transition: while protamine incorporation is perturbed in some of nuclei, many SD^+ spermatids progress through spermiogenesis and are eventually released in the seminal vesicles. Our study reveals for the first time that these mature SD^+ spermatozoa have improperly compacted nuclei despite their apparent normal shape. Although we know that these sperm cannot give rise to viable progeny, the timing of their elimination remains to be determined.

A remarkable and well-established feature of *SD* is the positive correlation between *Rsp* copy number and sensitivity to distortion (Wu *et al.,* 1988; Pimpinelli and Dimitri, 1989). Our study of several sensitive SD^+ chromosomes reveals that the correlation also extends to the cytological phenotypes. For chromosomes with >2000 *Rsp* copies (Rsp^{ss} chromosomes), spermatid elimination occurs at individualization, while spermatids carrying second chromosomes with fewer *Rsp* copies ($\leq$1300; Rsp^{s} chromosomes) tend to escape this differentiation arrest. These results support the hypothesis that a very large *Rsp* satDNA block perturbs the histone-to-protamine transition in distorter males, likely by impeding local SNBP deposition and normal chromatin compaction. In distorter males carrying a Rsp^{ss} chromosome, compaction defects in SD^+ spermatids might reach a threshold that triggers their systematic elimination during the individualization process. Supporting a functional link between *SD* and SNBPs, knocking-down *Mst35Ba/b* or *Mst77F* induces segregation distortion in the absence of the *Sd* mutation but in the presence of the other *SD* genetic components [i.e *M(SD); E(SD)* and *St(SD)*] (Gingell and McLean, 2020). This observation suggests that limiting amounts of SNBPs in a sensitized genetic background exacerbate the negative impact of the Rsp^{ss} satDNA on sperm nuclear compaction.

It is still unclear how *Rsp* satDNA perturbs the histone-to-protamine transition. Several studies suggest that spermatid differentiation defects may result from perturbation of *Rsp* satDNA

transcriptional activity and/or chromatin state early during pre-meiotic stages. For instance, although the *SD* phenotype manifests post meiosis, the critical stage for the establishment of distortion is in spermatocytes (Mange, 1968; but see Matthews and Mortin, 1983) and the main driver, *Sd-RanGAP,* was shown to be mislocalized in primary spermatocytes (Kusano *et al.,* 2001). Moreover, the piRNA pathway, which is active early in spermatogenesis (Nishida *et al.,* 2007; Nagao *et al*., 2010, Quénerch'du *et al*., 2016), may also influence *SD* through its role in regulating repeated DNA by recruiting proteins involved in establishing heterochromatin such as the H3K9 methyltransferase Eggless/SETDB1 (Sienski *et al.*, 2015; Sato and Siomi, 2020). Indeed, several heterozygous mutants of piRNA biogenesis pathway genes enhance distortion levels in the *SD* system (Gell and Reenan, 2013). In addition, the piRNA pathway regulates transcription of *Rsp* in testes and ovaries (Chen *et al*., 2020 preprint; Wei *et al*., 2020 preprint) and influences heterochromatin establishment at *Rsp* satDNA in embryos (Wei *et al*., 2020 preprint). Thus, *Rsp* piRNA biogenesis may be disrupted in distorter males. For example, a mislocalized Sd-RanGAP protein may perturb the nucleo-cytoplasmic trafficking of precursor RNAs and then leads to defective *Rsp* heterochromatin establishment and/or maintenance in premeiotic cells (Tao *et al.,* 2007; Ferree and Barbash, 2007; Gell and Reenan, 2013). The resulting aberrant heterochromatin organization could locally disturb histone eviction and/or SNBP incorporation in elongating spermatids. Interestingly, downregulating non-coding RNAs from the most abundant satDNA in the *D. melanogaster* genome, (AAGAG)n, in premeiotic cells, perturbs Mst77F and ProtA/B incorporation and blocks spermatid differentiation (Mills *et al.* 2019). This study thus supports the notion that satDNA transcription is essential early during spermatogenesis, possibly to produce piRNA and maintain heterochromatin, to allow normal progression of spermatid nuclei through the histone-to-protamine transition. The repetitive nature of satDNA sequences may make them intrinsically difficult to pack with SNBPs and this could require a proper heterochromatin organization. However, as piRNA functions in the fly testes remain poorly understood (Quénerch'du

et al., 2016), we cannot exclude the possibility that satDNA piRNAs play a direct role in the histone-to-protamine transition.

It has been previously proposed that spermatid individualization may represent a checkpoint to eliminate improperly differentiated spermatids (McKee, 1998; Steinhauer, 2015; Kimura and Loppin, 2016). Perturbation of this process has been observed in other genetic backgrounds, such as in *Mst77F* loss-of-function mutants for instance (Kimura and Loppin, 2016). In *Gla/SD5, Gla/SD-Mad* and *RAL-380/SD-Mad* males, the systematic and rapid SD^+ Rsp^{ss} spermatid degeneration at the time of individualization strongly implies that this is an active process. Supporting the checkpoint hypothesis, we occasionally observed abnormally-compacted spermatid nuclei being eliminated during individualization in wildtype flies (data not shown). Similarly, Tokuyasu and colleagues reported the presence of abnormal spermatids that fail to individualize in wildtype flies like SD^+ spermatids in *SD*/SD^+ males (Tokuyasu *et al.,* 1972). The checkpoint may function to selectively remove abnormal spermatids, thus avoiding the production of defective spermatozoa that could impact progeny survival.

We propose that the individualization checkpoint could be activated when spermatid nuclei are not properly compacted. In our model, perturbation of the histone-to-protamine transition locally in the chromatin within the large block of *Rsp* satDNA could trigger the arrest of SNBP incorporation in the whole nucleus and its elimination (Figure 8). This model could explain why SD^+ Rsp^s (with $\leq$ 1300 repeats) spermatids are not systematically eliminated at individualization. In this case, protamine incorporation and thus nuclear compaction would be less disturbed and might be sufficient in some nuclei to escape the checkpoint. A similar mechanism may also be involved in some interspecific hybrids where male sterility is apparently caused by defective heterochromatin state in pre-meiotic cells that result in post-meiotic defects (Kulathinal and Singh, 1998; Bayes and Malik, 2009) or in other meiotic drive systems (Courret *et al*., 2019).

SD is a co-adapted gene complex that involves several linked enhancers of drive (Ganetzky, 1977; Sandler and Hiraizumi, 1960; Hiraizumi *et al.,* 1980; Brittnacher and Ganetzky, 1984; Sharp *et al.,* 1985; Temin, 1991; Larracuente and Presgraves, 2012) and both linked and unlinked suppressors that counteract drive (Hiraizumi *et al*., 1984; Trippa and Loverre, 1975; Courret *et al.,* 2019; Larracuente and Presgraves, 2012; Greenberg Temin, 2020). While the existence and contribution of these genetic factors to levels of distortion is well documented, it seems also important to consider their impact on spermiogenesis. For instance, we have identified a weak suppressor, *Su(SD)X-380,* which substantially modifies the phenotype of spermatid elimination with a modest effect of segregation distortion levels.

Finally, beyond the interest of understanding meiotic drive systems in general, this work shows that *SD* is an excellent model to study spermiogenesis and the constraint of heterochromatin organization on the histone-to-protamine transition. Future work characterizing the chromatin organization and transcriptional activity of the *Rsp* satDNA should yield important insights into drive and spermatogenesis.

Materials and Methods

Fly genetics

Flies were reared at 25°C on a classical agar, yeast, corn flour fly medium. The following strains were obtained from the Bloomington Drosophila Stock Center (BDSC) and used as a source of Rsp^{s} chromosomes: *Gla/CyO* [w^{1118}; *In(2LR)Gla,* wg^{Gla-1} Bc^{1}/*CyO*; stock #5439], *iso-1* or cn^{1} bw^{1} [y^{1}; $Gr22b^{iso-1}$ $Gr22d^{iso-1}$ cn^{1} $CG33964^{iso-1}$ bw^{1} sp^{1}; $MstProx^{iso-1}$ $GstD5^{iso-1}$ $Rh6^{1}$; stock #2057], *RAL-380* (stock #25190), *RAL-313* (stock #25180), *RAL-309* (stock #28166). The two following stocks carrying the strong *SD5* and *SD-Mad* distorter chromosomes were also obtained from the BDSC: *SD5/SM1* [*In(2R)SD5, In(2R)NS, Dp(2;2)*$RanGAP^{SD}$, $RanGAP^{SD}$/*SM1; stock* #393] and *SD-Mad* [*SD-Mad, In(2LR)SD72, In(2R)NS, Dp(2;2)*$RanGAP^{Sd}$, $RanGAP^{Sd}$ $E(SD)^{1}$ Rsp^{i} $M(SD)^{1}$ $St(SD)^{1}$;

#64324]. The *protB-GFP* transgene was previously described (Jayaramaiah Raja and Renkawitz-Pohl, 2005). To obtain *SD* males carrying *protB-GFP*, we generated the two stocks: w^{1118}*; SD-Mad/CyO; protB-GFP/TM6B* and w^{1118}*; SD5/CyO; protB-GFP/TM6B.* Males from these stocks were crossed to w^{1118}*; Gla/CyO* or *y;* cn^1 bw^1 virgin females to obtain distorter males.

To test distortion on the RAL strain second chromosomes, we first generated a marked *SD* chromosome with a *Cy* dominant marker. After meiotic recombination between *Cy Kr* and *SD-Mad* chromosomes, a strong *Cy* distorter recombinant chromosome was selected and backcrossed several times with *SD-Mad*. Since *Cy SD-Mad* is maintained in heterozygous background with *SD-Mad*, we select flies with *Cy SD-Mad* chromosome every generation (see cross scheme on Figure S8).

Distortion genetic tests and k-value

To measure genetic distortion levels, single males (2–5 days old) were crossed with two virgin females and placed at 25°C for one week before discarding the flies. For each genotype tested, 10 to 20 independent crosses were set up. In each vial, the progeny was genotyped and counted for 18 days after parents were introduced in the vial. Crosses producing less than 30 flies were not considered. The strength of segregation distortion is expressed as a *k* value, calculated as the number of flies carrying the *SD* chromosome (or the control chromosome, see Table 1) among the total progeny.

Immunofluorescence on whole mount testes

Testes from 2 to 5-day old males were dissected in PBS-T (1X PBS, 0.15% Triton) and fixed for 20 min in 4 % formaldehyde at room temperature. Testes were washed three times in PBS-T and incubated with primary antibody overnight at 4°C. After three 20-min washes in PBS-T, they were incubated with secondary antibodies at room temperature for 2 hours. They were then washed three times and mounted in mounting medium (DAKO, ref #S3023) containing 1µg/mL DAPI or incubated with Phalloidin 633 (1:1000 in 1X-PBS; Phalloidin-FluoProbes 633A #FT-FP633A) for

30 min at room temperature, washed and mounted in the DAPI mounting medium. Primary antibodies used were: mouse anti-histone antibody (1:1000; Millipore ref # MABE71), rabbit Tpl94D (1:100; Kimura and Loppin, 2016), mouse anti-dsDNA (1:3000, Abcam ref # 27156), rabbit anti-Vasa (1: 5000; a generous gift from Paul Lasko, McGill University, Canada) and secondary antibodies were a DyLight 550 conjugated goat anti-rabbit IgG (ThermoScientific; ref#84541) and DyLight 550 conjugated goat anti-mouse IgG (ThermoScientific; ref#84540). Images were acquired on an LSM800 confocal microscope (CarlZeiss) and processed using the Zen (CarlZeiss) and Fiji softwares (Schindelin *et al.,* 2012). For each experiment at least three independent crosses and immunostainings of 5–7 testis pairs were done.

DNA-FISH

DNA-FISH of *Rsp* and *359 bp* satellites on testes from *SD-Mad/cn*^{1} *bw*^{1} males were performed following Larracuente and Ferree (2015). Testes from 3–5 day old flies were dissected in PBS and treated for 8 min in 0.5% sodium citrate. The testes were fixed in 45% acetic acid and 2% formaldehyde for 6 min, placed on a poly-L-lysine slide, squashed, and dehydrated. Slides were denatured at 95°C for 5 min in hybridization buffer (with *Rsp* and *359 bp* satellite probes) and incubated at 37°C overnight in a humid chamber. The *Rsp* probe was a Stellaris probe from (Chang *et al*., 2019; Wei *et al*., 2020 preprint; Rsp-Quasar570) and the *359 bp* probe was a Cy5-labeled oligo probe (5'-Cy5TTTTCCAAATTTCGGTCATCAAATAATCAT-3') previously described in Ferree and Barbash (2009). Slides were mounted in SlowFade™ Diamond Antifade Mountant with DAPI (ThermoFisher ref # S36964), visualized on a Leica DM5500 upright fluorescence microscope, imaged with a Hamamatsu Orca R2 CCD camera, and analyzed using Leica's LAX software.

For DNA-FISH on squashed testes from *Gla/SD5* males (Figure 1) and seminal vesicles (Figure 5), probes were prepared as follows. A 359 bp fragment from the *359 bp* satDNA on the X chromosome

was PCR amplified using the following primers 5'-CGGTCATCAAATAATCATTTATTTTGC-3' and 5'-CGAAATTTGGAAAAACAGACTCTGC-3' (Dernburg, 2011) and w^{1118} genomic DNA as a template. The fragment was then cloned using T/A cloning in the pGEMT vector (Promega, ref#A1360). For the *Rsp* satDNA probe, we amplified the *Rsp* satDNA by PCR from *Gla/CyO* genomic DNA and cloned a ca. 700bp fragment corresponding to about four *Rsp* repeats in a pGEMT vector. Primer used were 5'-CCAGGCGAACAGAAGATACC-3' et 5'-TTTTGACCGCTTAAAATGACA-3'. *359 bp* and *Rsp* pGEMT plasmids were then used as templates to synthetize DNA probes using, respectively, the PCR labelling Cy-3 and Cy-5 kits (Jena Bioscience, ref# PP-301L-Cy3 and #APP-101-Cy5) according to the manufacturer's instructions with M13 universal primers. Spermatozoa spreads were prepared as described in (Tirmarche *et al.*, 2016) with modifications. Seminal vesicles from 4 to 5-day old males were dissected in PBS, then opened with needles to spread sperm cells on home-made polyL-lysine coated slides. Spermatozoa were then permeabilized in 1% Triton-PBS for 30 min at room temperature, treated with 2mM DTT in PBS for 30 min to reduce disulfide bonds, washed twice with PBS and incubated in fixation solution (50% acetic acid, 4% formaldehyde in PBS) for 4 min at room temperature. The slides were then dehydrated in absolute ethanol, air dried and kept at 4°C until staining. For squashed testes, tissues were dissected in PBS-0.15% Triton, incubated for 4 min in a drop of fixation fixative solution, squashed and frozen in liquid nitrogen. Slides were then dehydrated for 10 min in absolute ethanol and air dried.

DNA-FISH was then performed as described in (Cazemajor *et al.,* 2000) with modifications. Slides were rehydrated in PBS for 5 min at RT, then incubated in 100mM HCl/0.1% pepsin for 90 seconds to remove proteins, washed in PBS and incubated in a 3:1ethanol/acetic acid mix for 15 min at RT. Then slides were rinsed in 2X SSC, treated with 0.2 mg/mL RNaseA in 2X SSC for 30 min at 37°C and rinsed again with 2X SSC before dehydration in successive 70%, 90% and 100% ethanol baths and air dried. Sperm cells were first incubated in a drop of 70% formamide/2X SSC and incubated

at 95°C for 5 min. After denaturation, the slides were washed twice with ice cold 2X SSC for two min, dehydrated and air dried. The probes (50 ng of *Rsp* and 35 ng of *359 bp* probes per slide) were diluted in hybridization buffer (1mg/mL sonicated salmon sperm DNA (Sigma-Aldrich ref# D9156), 50% formamide, 2X SSC, 50 % Dextran Sulfate). The mixture was boiled at 95°C for 5 min and quickly chilled on ice before deposition on sperm nuclei. The slides were incubated at 37°C overnight. After hybridization, the slides were washed three times in 2X SSC at 42°C for 5 min, and once in 0.2X SSC for 5 min at room temperature. They were then air dried before adding mounting medium containing 1µg/mL DAPI. Images were acquired as described for Immunofluorescence.

Quantitative PCR

Genomic DNA from 5 males was extracted using the NucleoSpin Tissue XS kit (Macherey-Nagel, ref #740 901). To amplify the *Rsp* satDNA region, we used two sets of primers: 5'-CCAGGCGAACAGAAGATACC-3' and 5'-TTTTGACCGCTTAAAATGACA-3'; and 5'-AAGTTATGTCATTTTAAGCGGTCA-3' and 5'-AACTTAGGCAATTTACTGTTTTTGC-3'. As a control, we amplified a fragment into *nup62* gene (primers 5'-GGCACCTACTGCTGGTATCG-3' and 5'-AATCCAAAGGCTGGTGGAG-3'). Quantitative PCR analysis was performed with 5ng of template gDNA in a 25µl reaction using the TB Green Premix Ex Taq II (Takara, #RR820L) and the CFX Connect (Biorad CFX Connect) system. For each set of primers, standard and melting curve analyses were performed to check for, respectively, PCR efficiency and specificity. qPCR analysis was done using technical duplicates on three biological replicates. The *nup62* gene was used as internal control with a known copy number (2) so that genomic DNA levels were normalized for each sample to the levels of *nup62*. Based on Khost *et al.* (2017), we considered that cn^1 bw^1/*SD-Mad* flies carry 1000 repeats. The copy number in the *Rsp* satDNA is relative to cn^1 bw^1/ *SD-Mad* and was calculated using the comparative quantification ΔΔCT method (Livak and Schmittgen, 2001).

Acknowledgments

We are grateful to the Bloomington Drosophila Stock Center and the Drosophila Genetic Reference Panel for fly stocks and to the SFR Biosciences (UMS3444/CNRS, US8/Inserm, ENS de Lyon, UCBL) facilities: Robert Renard and the Arthro-Tools staff for fly food preparation and the Plateau Technique d'Imagerie/Microscopie. We thank Hafida Sellou for her help in the preliminary observation of SD male phenotypes, Paul Lasko for kindly providing the anti-Vasa antibody, Marie Delattre for the Cy3 labeling kit, Guillermo Orsi and Béatrice Horard for critical reading of the manuscript and Loppin's lab for discussion and feedback.

Competing interest

The authors declare no competing interests

Funding

This work was supported by a grant to RD from the Agence Nationale de La Recherche (ANR-16-CE12-0006-01) and a grant to AML from the National Institutes of Health (R35 GM119515).

References

Bayes, J. J. and Malik, H. S. (2009). Altered heterochromatin binding by a hybrid sterility protein in Drosophila sibling species. *Science*. 326(5959):1538-1541. doi:10.1126/science.1181756

Bonnefoy, E., Orsi, G. A., Couble ,P., Loppin B. (2007). The essential role of Drosophila HIRA for de novo assembly of paternal chromatin at fertilization. *PLoS Genet*. 3(10):1991-2006. doi:10.1371/journal.pgen.0030182

Brittnacher, J.G. and Ganetzky, B. (1983). On the Components of Segregation Distortion in *Drosophila melanogaster*. II. Deletion Mapping and Dosage Analysis of the SD Locus. *Genetics*. 103(4):659-73

Brittnacher, J. G. and Ganetzky, B. (1984) On the components of segregation distortion in Drosophila melanogaster. III. Nature of enhancer of SD. *Genetics*. 107(3):423-34.

Cazemajor, M., Joly, D. and Montchamp-Moreau, C. (2000). Sex-ratio meiotic drive in Drosophila simulans is related to equational nondisjunction of the Y chromosome. *Genetics*. 154(1):229-236.

Chang, C. H., Chavan, A., Palladino, J., Wei, X., Martins, N. M. C., Santinello, B., Chen, C. C., Erceg, J., Beliveau, B. J., Wu, C. T., Larracuente, A. M. and Mellone, B. G. (2019). Islands of retroelements are major components of Drosophila centromeres. *PLoS Biol.* 17(5):e3000241. doi: 10.1371/journal.pbio.3000241.

Chen, P., Luo., Y. and Aravin, A. A. (2020). RDC complex executes a dynamic piRNA program during *Drosophila* spermatogenesis to safeguard male fertility. *bioRxiv*. doi: https://doi.org/10.1101/2020.08.25.266643

Courret, C., Chang, C. H., Wei, K. H., Montchamp-Moreau, C. and Larracuente, A. M. (2019). Meiotic drive mechanisms: lessons from *Drosophila*. *Proc Biol Sci*. 286(1913):20191430. doi:10.1098/rspb.2019.1430

Dernburg, A. F. (2011). In situ hybridization to somatic chromosomes in Drosophila. *Cold Spring Harb Protoc*. (9) :pdb.top065540. doi:10.1101/pdb.top065540

Doyen, C. M., Chalkley, G. E., Voets, O., Bezstarosti, K., Demmers, J. A., Moshkin Y. M. and Verrijzer, C. P. (2015). A Testis-Specific Chaperone and the Chromatin Remodeler ISWI Mediate Repackaging of the Paternal Genome. *Cell Rep*. 13(7):1310-1318. doi:10.1016/j.celrep.2015.10.010.

Eren-Ghiani, Z., Rathke, C., Theofel, I. and Renkawitz-Pohl, R. (2015). Prtl99C Acts Together with Protamines and Safeguards Male Fertility in Drosophila. *Cell Rep*. 13(11):2327-2335. doi:10.1016/j.celrep.2015.11.023

Fabian, L. and Brill, J. A. (2012). Drosophila spermiogenesis: Big things come from little packages. *Spermatogenesis*. 2(3):197-212. doi:10.4161/spmg.21798

Ferree, P. M. and Barbash, D. A. (2007). Distorted sex ratios: a window into RNAi-mediated silencing. *PLoS Biol*. 5(11):e303. doi:10.1371/journal.pbio.0050303

Ferree, P. M. and Barbash, D. A. (2009). Species-specific heterochromatin prevents mitotic chromosome segregation to cause hybrid lethality in Drosophila. *PLoS Biol.* 7(10):e1000234. doi: 10.1371/journal.pbio.1000234.

Fuller MT (1993). Spermatogenesis. In: Bate M, Martinez Arias A, editors. The development of Drosophila melanogaster. 1 ed. Cold Spring Harbor, NY: Cold Spring Harbor Laboratory Press. pp. 71–148.

Ganetzky, B. (1977). On the components of segregation distortion in Drosophila melanogaster. *Genetics*. 86(2 Pt. 1), 321–355.

Gell, S. L. and Reenan, R. A. (2013). Mutations to the piRNA pathway component aubergine enhance meiotic drive of segregation distorter in Drosophila melanogaster. *Genetics*. 193(3):771-784. doi:10.1534/genetics.112.147561

Gingell, L. F. and McLean, J. R. (2020). A Protamine Knockdown Mimics the Function of *Sd* in *Drosophila melanogaster*. *G3 (Bethesda)*. 10(6):2111-2115. doi: 10.1534/g3.120.401307.

Greenberg Temin, R. (2020). Analysis of a Strong Suppressor of Segregation Distorter in *Drosophila melanogaster*. *Genetics*. 215(4):1085-1105. doi:10.1534/genetics.120.303150.

Hauschteck-Jungen, E. and Hartl, D. L. (1982). Defective Histone Transition during Spermiogenesis in Heterozygous Segregation Distorter males of *Drosophila melanogaster*. *Genetics*. 101(1):57-69.

Hiraizumi, Y., Martin, D. W. and Eckstrand, I. A. (1980). A Modified Model of Segregation Distortion in Drosophila melanogaster. *Genetics*. 95(3):693-706.

Huang, W., Massouras, A., Inoue, Y., Peiffer, J., Ràmia, M., Tarone, A. M., Turlapati, L., Zichner, T., Zhu, D., Lyman, R.F *et al.* (2014). Natural variation in genome architecture among 205 *Drosophila melanogaster* Genetic Reference Panel lines. *Genome Res.* 24(7):1193-208. doi: 10.1101/gr.171546.113.

Jayaramaiah Raja, S. and Renkawitz-Pohl, R. (2005). Replacement by Drosophila melanogaster protamines and Mst77F of histones during chromatin condensation in late spermatids and role of sesame in the removal of these proteins from the male pronucleus. *Mol Cell Biol*. 25(14):6165-6177. doi:10.1128/MCB.25.14.6165-6177.2005

Kimura, S. and Loppin, B. (2016). The Drosophila chromosomal protein Mst77F is processed to generate an essential component of mature sperm chromatin. *Open Biol*. 6(11):160207. doi:10.1098/rsob.160207

Khost, D. E., Eickbush, D. G. and Larracuente, A. M. (2017). Single-molecule sequencing resolves the detailed structure of complex satellite DNA loci in *Drosophila melanogaster*. *Genome Res*. 27(5):709-721. doi:10.1101/gr.213512.116

Kulathinal, R. and Singh, R. S. (1998). Cytological characterization of premeiotic versus postmeiotic defects producing hybrid male sterility among sibling species of the *Drosophila melanogaster* complex. *Evolution.* 52(4):1067-1079. doi: 10.1111/j.1558-5646.1998.tb01834.x.

Kusano, A., Staber, C. and Ganetzky B. (2001). Nuclear mislocalization of enzymatically active RanGAP causes segregation distortion in Drosophila. *Dev Cell*. 1(3):351-361. doi:10.1016/s1534-5807(01)00042-9

Larracuente, A. M. and Ferree, P. M. (2015). Simple method for fluorescence DNA in situ hybridization to squashed chromosomes. *JoVE*. (95), 52288. https://doi.org/10.3791/52288

Larracuente, A. M. and Presgraves, D. C. (2012). The selfish Segregation Distorter gene complex of Drosophila melanogaster. *Genetics*. 192(1):33-53. doi:10.1534/genetics.112.141390

Lewis, J. D., Song, Y., de Jong, M. E., Bagha, S.M. and Ausió, J. (2003). A walk though vertebrate and invertebrate protamines. *Chromosoma*. 111(8):473-482. doi:10.1007/s00412-002-0226-0

Lindholm, A. K., Dyer, K. A., Firman, R. C., Fishman, L., Forstmeier, W., Holman, L., Johannesson, H., Knief, U., Kokko, H., Larracuente, A. M. *et al.* (2016). The Ecology and Evolutionary Dynamics of Meiotic Drive. *Trends Ecol Evol*. 31(4):315-326. doi:10.1016/j.tree.2016.02.001

Livak, K. J. and Schmittgen, T. D. (2001). Analysis of relative gene expression data using real-time quantitative PCR and the 2(-Delta Delta C(T)) Method. *Methods.* 25(4):402-8. doi: 10.1006/meth.2001.1262

Lyttle, T. W. (1991). Segregation distorters. *Annu Rev Genet*. 25:511-557. doi:10.1146/annurev.ge.25.120191.002455

Mackay, T. F., Richards, S., Stone, E. A., Barbadilla, A., Ayroles, J. F., Zhu, D., Casillas, S., Han, Y., Magwire, M. M., Cridland, J. M. et al. (2012). The *Drosophila melanogaster* Genetic Reference Panel. *Nature.* 482(7384):173-8. doi: 10.1038/nature10811.

Mange, E. J. (1968). Temperature sensitivity of segregation-distortion in Drosophila melanogaster. *Genetics*, *58*(3), 399–413.

Matthews, K. and Mortin, M. A. (1983). SD-72 as a temperature-sensitive period during spermiogenesis. *Can. J. Genet. Cytol.* 25:662-667.

McKee, B. D. (1998). Pairing sites and the role of chromosome pairing in meiosis and spermatogenesis in male Drosophila. *Curr Top Dev Biol*. 37:77-115. doi:10.1016/s0070-2153(08)60172-6

Merrill, C., Bayraktaroglu, L., Kusano, A. and Ganetzky B. (1999). Truncated RanGAP encoded by the Segregation Distorter locus of Drosophila. *Science*. 283(5408):1742-1745. doi:10.1126/science.283.5408.1742

Mills, W. K., Lee, Y. C. G., Kochendoerfer, A. M., Dunleavy, E. M. and Karpen, G. H. (2019). RNA from a simple-tandem repeat is required for sperm maturation and male fertility in *Drosophila melanogaster*. *Elife*. 8:e48940. Published 2019 Nov 5. doi:10.7554/eLife.48940

Nagao, A., Mituyama, T., Huang, H., Chen, D., Siomi, M. C. and Siomi H. (2010). Biogenesis pathways of piRNAs loaded onto AGO3 in the Drosophila testis. *RNA*. 16(12):2503-2515. doi:10.1261/rna.2270710

Nishida, K. M., Saito, K., Mori, T., Kawamura, Y., Nagami-Okada, T., Inagaki, S., Siomi, H. and Siomi M. C. (2007). Gene silencing mechanisms mediated by Aubergine piRNA complexes in Drosophila male gonad. *RNA.* 13(11):1911-22. doi: 10.1261/rna.744307.

Pimpinelli, S. and Dimitri, P. (1989). Cytogenetic analysis of segregation distortion in Drosophila melanogaster: the cytological organization of the Responder (Rsp) locus. *Genetics*. 121(4):765-772.

Peacock, W. J. and Erickson, J. (1965). Segregation-Distortion and regularly nonfunctional products of spermatogenesis in Drosophila melanogaster. *Genetics*. 51(2):313-328.

Powers, P. A. and Ganetzky, B. (1991). On the components of segregation distortion in Drosophila melanogaster. V. Molecular analysis of the Sd locus. *Genetics*. 129(1):133-144.

Presgraves, D. C., Gérard, P. R., Cherukuri, A. and Lyttle, T. W. (2009). Large-scale selective sweep among Segregation Distorter chromosomes in African populations of Drosophila melanogaster. *PLoS Genet*. 5(5):e1000463. doi:10.1371/journal.pgen.1000463

Quénerch'du, E., Anand, A. and Kai, T. (2016). The piRNA pathway is developmentally regulated during spermatogenesis in Drosophila. *RNA*. 22(7):1044-1054. doi:10.1261/rna.055996.116

Rathke, C., Baarends, W. M., Awe, S. and Renkawitz-Pohl, R. (2014). Chromatin dynamics during spermiogenesis. *Biochim Biophys Acta*. 1839(3):155-168. doi:10.1016/j.bbagrm.2013.08.004

Rathke, C., Baarends, W.M., Jayaramaiah-Raja S., Bartkuhn M., Renkawitz R. and Renkawitz-Pohl R. (2007). Transition from a nucleosome-based to a protamine-based chromatin configuration during spermiogenesis in Drosophila. *J Cell Sci*. 120(Pt 9):1689-1700. doi:10.1242/jcs.004663

Sandler, L., Hiraizumi, Y. and Sandler, I. (1959). Meiotic Drive in Natural Populations of Drosophila Melanogaster. I. the Cytogenetic Basis of Segregation-Distortion. *Genetics*. 44(2):233-250.

Sandler, L. and Hiraizumi, Y. (1960). Meiotic Drive in Natural Populations of Drosophila Melanogaster. IV. Instability at the Segregation-Distorter Locus. *Genetics*, *45*(9), 1269–1287.

Sato, K. and Siomi, M. C. (2020). The piRNA pathway in Drosophila ovarian germ and somatic cells. *Proc Jpn Acad Ser B Phys Biol Sci.* 96(1):32-42. doi: 10.2183/pjab.96.003.

Schindelin, J., Arganda-Carreras, I., Frise E., Kaynig, V., Longair, M., Pietzsch, T., Preibisch, S., Rueden, C., Saalfeld, S., Schmid, B. *et al.* (2012). Fiji: an open-source platform for biological-image analysis. *Nat Methods*. 9(7):676-682. doi:10.1038/nmeth.2019

Sharp, C. B., Hilliker, A. J. and Holm, D. G. (1985). Further characterization of genetic elements associated with the segregation distorter phenomenon in Drosophila melanogaster. *Genetics* **110**: 671--688.

Sienski, G., Batki, J., Senti, K. A., Dönertas, D., Tirian, L., Meixner, K. and Brennecke J. (2015) Silencio/CG9754 connects the Piwi-piRNA complex to the cellular heterochromatin machinery. *Genes Dev.* 29(21):2258-71. doi: 10.1101/gad.271908.115

Steggerda, S. M. and Paschal, B. M. (2002). Regulation of nuclear import and export by the GTPase Ran. *Int Rev Cytol*. 217:41-91. doi:10.1016/s0074-7696(02)17012-4

Steinhauer, J. (2015). Separating from the pack: Molecular mechanisms of *Drosophila* spermatid individualization. *Spermatogenesis*. 5(2):e1041345. doi:10.1080/21565562.2015.1041345

Tao, Y., Masly, J.P., Araripe, L., Ke, Y. and Hartl, D.L. (2007). A sex-ratio meiotic drive system in *Drosophila simulans*. I: an autosomal suppressor. *PLoS Biol*. 5(11):e292. doi:10.1371/journal.pbio.0050292

Temin, R. G. (1991). The independent distorting ability of the Enhancer of Segregation Distortion, E(SD), in Drosophila melanogaster. *Genetics.* 128(2):339-56.

Tirmarche, S., Kimura, S., Dubruille, R., Horard, B. and Loppin, B. (2016). Unlocking sperm chromatin at fertilization requires a dedicated egg thioredoxin in Drosophila. *Nat Commun*. 7:13539. doi:10.1038/ncomms13539

Tokuyasu, K. T., Peacock, W. J. and Hardy, R. W. (1972). Dynamics of spermiogenesis in Drosophila melanogaster. I. Individualization process. *Z Zellforsch Mikrosk Anat.* 124(4):479-506. doi: 10.1007/BF00335253. PMID: 4622067.

Tokuyasu, K. T., Peacock, W. J. and Hardy, R. W. (1977). Dynamics of spermiogenesis in Drosophila melanogaster. VII. Effects of segregation distorter (SD) chromosome. *J Ultrastruct Res*. 58(1):96-107. doi:10.1016/s0022-5320(77)80011-7

Trippa, G. and Loverre, A. (1975). A factor on a wild third chromosome (IIIRa) that modifies the segregation distortion phenomenon in Drosophila melanogaster. *Genet Res*. 26(2):113-25. doi: 10.1017/s0016672300015925.

Wei X., Eickbush, D. G., Speece, I. and Larracuente, A. M. (2020). Heterochromatin-dependent transcription of satellite DNAs in the *Drosophila melanogaster* female germline. *bioRxiv* doi: https://doi.org/10.1101/2020.08.26.268920

Wu, C. I., Lyttle, T. W., Wu, M. L. and Lin, G. F. (1988). Association between a satellite DNA sequence and the Responder of Segregation Distorter in D. melanogaster. *Cell*. 54(2):179-189. doi:10.1016/0092-8674(88)90550-8

Figure legends

Figure 1: In *SD* males, cytological defects are observed at the end of spermiogenesis, during the histone-to-protamine transition.

(A) The two main genetic elements involved in *SD* on the second chromosome. *Sd* is a duplication of the *RanGAP* gene and its target is the *Rsp* satDNA on the homologous chromosome. Gray boxes represent pericentric heterochromatin. Other uncharacterized genetic elements (*Enhancer of SD [E(SD)]; Modifier of SD [M(SD)] and Stabilizer of SD [St(SD)]*) located on SD chromosomes are also required to induce high levels of distortion (Ganetsky, 1977; Sandler and Hiraizumi 1960; Hiraizumi *et al.,* 1980; Larracuente and Presgraves, 2012) (B) A scheme of a fly testis showing the organization of spermatogenesis. Spermatogenesis starts at the apical tip and progresses along the tubular axis of the fly testis (Fuller, 1993). Germ stem cells divide asymmetrically to form another germ stem cell and a spermatogonium. After four incomplete mitoses without cytokinesis, the 16 primary spermatocytes of each cyst enter meiosis and produce 64 round spermatids which are interconnected with cytoplasmic bridges and surrounded by two cyst cells (not represented on the scheme). The 64 spermatids then differentiate into mature sperm cells in synchrony. Round spermatid nuclei elongate to form needle-shaped nuclei. During this nuclear reshaping and remodeling, almost all histones (red) are removed and replaced by transition proteins (yellow) such as Tpl94D, which are then also eliminated and replaced by Mst35Ba/b, Mst77F and Prtl99 (green) during the histone-to-protamine transition. At the end of spermiogenesis, spermatids individualized and coiled before being released in the seminal vesicle. (C) Confocal images of whole-mount fly testes from a control *Gla/CyO; protB-GFP* male (top) and a distorter *Gla/SD5; protB-GFP* male (bottom) stained with DAPI (blue), and antibodies against histones (red) and Vasa (white). In distorter males, spermatogonial amplification and meiosis appear normal and the first cytological

defects are observed during the histone-to-protamine transition. In many cysts, about half of the nuclei are abnormally shaped and eliminated. Scale bar: 100µm in large views and 20µm in magnified squares. (D) Cysts of 64 spermatids of the indicated genotypes. In *Gla/SD5; protB-GFP* testes (bottom panel), about half spermatid nuclei appear abnormally shaped are eliminated (arrow). Scale bar: 10µm. (E) DNA-FISH staining of squashed testes with specific probes for *Rsp* (green) and *359 bp* satDNA on the X chromosome (red). In *Gla/SD5*, the abnormally-shaped spermatid nuclei that are eliminated carry the second chromosome with the large *Rsp* satDNA block. In cn^1 bw^1*/SD-Mad*, abnormally-shaped spermatid nuclei carry a second chromosome with a large *Rsp* satDNA block. A few spermatid nuclei stained with the *Rsp* probe are normally shaped (arrowheads). Scale bar: 10µm.

Figure 2: Histone elimination and Tpl94D transient expression is slightly delayed in *Gla/SD5* males.

Confocal images of whole-mount testes from males stained with a pan-histone antibody (red), an antibody against the Tpl94D transition protein (white) and for DNA (DAPI, cyan). Each image shows one or two cysts of 64 spermatid nuclei at the indicated stage of the transition that was estimated with nuclear shape and staining intensity for each signal. In control *Gla/CyO* males, spermatids nuclei which are positive for Tpl94D have almost lost all their histones (see oversaturated image on bottom panels, asterisks indicate somatic nuclei). At the end of spermiogenesis, all spermatid nuclei are negative for Tpl94D and histones. In *Gla/SD5* spermatids, traces of histones are detected in about half the nuclei in cysts that have incorporated Tpl94D (arrows, and oversaturated image below). Tpl94D staining is weaker in about half of the nuclei, compared to sister nuclei. However, at the end of spermiogenesis, all spermatid nuclei are negative for both histones and Tpl94D. In cn^1 bw^1*/ SD-Mad*, histone elimination and transient Tpl94D expression appear normal. Scale bar: 10µm.

Figure 3: Protamine incorporation is delayed in *Gla/SD5* and slightly disturbed in *cn*^{1} *bw*^{1}*/SD-Mad* testes

(A) A scheme of spermatid individualization. At the end of histone-to-protamine transition, actin cones form around each spermatid nuclei (individualization complex, IC) and progress along the flagellum to remove cytoplasmic excess. (B) Confocal images of whole-mount testes from males carrying a *protB-GFP* transgene (green) and stained with DAPI (blue) and phalloidin (F-actin, white), that reveals individualization complex (IC). Each square shows a cyst of 64 spermatid nuclei at the indicated stage [before individualization (pre-IC), at the onset of individualization (IC) and after individualization (post-IC)]. In control *Gla/CyO* males, ProtB-GFP fluorescence and nuclear shape appear homogeneous for the 64 spermatids at all stages. In *Gla/SD5* testes, about half of the nuclei show weaker ProtB-GFP signals in pre-IC cysts although nuclear shapes appear similar with DAPI staining. During individualization, the nuclei that present weaker GFP signals also appear larger (arrow). In post-IC stages, these nuclei are abnormally shaped (arrow) and eliminated in the waste bag. In *cn*^{1} *bw*^{1}*/SD-Mad* testes, this phenotype is weaker. In pre-IC and IC spermatids, ProtB-GFP signals are more homogeneous. In post-IC stages, only a few nuclei seem to be abnormally shaped (arrows). This phenotype is variable form one cyst to another and a *Gla/SD5*-like phenotype can be occasionally observed. Scale bar: 10µm. (C) A magnified view of a pre-IC cyst stained with DAPI showing a weaker ProtB-GFP signal in about half of spermatids.

Figure 4: *Rsp*^{s} spermatid are abnormally compacted in both *SD* genotypes

Confocal images of whole-mount testes from males carrying the *protB-GFP* transgene stained with an anti-dsDNA antibody (dsDNA-Ab; red) to probe for chromatin compaction, DAPI (blue) and phalloidin (not shown for clarity). In *Gla/CyO* control males, all nuclei in pre-IC cysts are homogenously and weakly stained with the anti-dsDNA antibody. When individualization starts

(IC) and after (post-IC), spermatid nuclei are not stained with the anti-dsDNA antibody because of the highly compacted chromatin becomes inaccessible to antibodies. In *Gla/SD5* pre-IC cysts, about half of the nuclei are more brightly stained with the anti-dsDNA antibody compared to their sister nuclei. This strong anti-dsDNA staining is negatively correlated to ProtB-GFP intensity signals. During individualization (IC), the abnormally shaped nuclei that are weakly stained with ProtB-GFP are also positively and brightly stained with the anti-dsDNA antibody (arrows). After individualization, the eliminated nuclei are also brightly stained with the anti-dsDNA antibody (arrows) whereas needle-shaped nuclei remain negative for this staining. In cn^1 bw^1*/SD-Mad* testes, spermatid nuclei in pre-IC cysts are homogeneously stained with the anti-dsDNA antibody except for a few nuclei which are more brightly stained (arrow). However, during individualization, some spermatid nuclei are brightly stained with the anti-dsDNA antibody (arrows, IC) and about half of the nuclei show a faint anti-dsDNA signal suggesting that most SD^+ nuclei are not normally compacted. Cysts of post-IC spermatids contain both abnormally-shaped and needle-shaped anti-dsDNA positive nuclei (arrow, post-IC). These latter nuclei are included in the bundle of *SD* spermatids, suggesting that they are not eliminated. Scale bar: 10µm.

Figure 5: Seminal vesicles of cn^1 bw^1 SD males contain many abnormally compacted Rsp^s nuclei

(A) Confocal images of whole-mount seminal vesicles from males of the indicated genotype, carrying the *protB-GFP* transgene (green) and stained with the anti-dsDNA antibody (dsDNA-Ab; red), DAPI (blue) and phalloidin (white). A wide view of the seminal vesicle is shown on left panels (scale bar: 50µm). Dashed white squares correspond to magnified regions shown on right panels (scale bar: 10µm). In cn^1 bw^1*/CyO* seminal vesicles, nearly all sperm nuclei are negative for the anti-dsDNA antibody. Seminal vesicles from cn^1 bw^1*/SD-Mad* and cn^1 bw^1*/SD5* males contain many anti-dsDNA positive sperm nuclei, suggesting that they are abnormally condensed although most of

them are needle-shaped and contain protamines. In *Gla/SD5* and *Gla/SD-Mad* seminal vesicles, such nuclei are rarely observed. Note that the seminal vesicles of *SD* males are smaller in general but *Gla/SD5* and *Gla/SD-Mad* vesicles are even smaller than *cn*^{1} *bw*^{1}*/SD5 and cn*^{1} *bw*^{1}*/SD-Mad* ones, indicating that they contain less sperm. (B) DNA-FISH performed on seminal vesicle contents of the indicated genotype with a *Rsp* probe (green) and a control probe for the *359 bp* satDNA (red) on the X chromosome as control (scale bar: 10µm). In all panels, sperm nuclei have been partially decondensed with DTT to facilitate probe penetration. In control *cn*^{1} *bw*^{1}*/CyO* seminal vesicles, about half of the nuclei are positive for the *Rsp* probe demonstrating that *SD*$^+$ *Rsp*^{s} spermatozoa are normally produced. In *cn*^{1} *bw*^{1}*/SD-Mad* and *cn*^{1} *bw*^{1}/SD5 seminal vesicles, many nuclei are positive for the *Rsp* probe, thus confirming that the anti-dsDNA positive sperm nuclei detected in seminal vesicles of these genotypes correspond to abnormal spermatozoa that inherited the *SD*$^+$ *Rsp*^{s} chromosome. (C) Box plot of the percentage of anti-dsDNA positive sperm nuclei in a Z-stack square as shown in middle panels in A. Whiskers show minimum and maximum values, boxes show the middle 50% of the values and horizontal lines represent medians. For each genotype, n indicates the number of seminal vesicles analyzed.

Figure 6: The cytological phenotype of SD males is linked to *Rsp* copy numbers

(A) *Rsp* copy numbers on the *Gla* chromosome and the second chromosome of *RAL* strains were estimated by qPCR on genomic DNA. For the quantification, two sets of *Rsp* primers were designed using the canonical *Rsp* left and right sequences published in Khost *et al.,* 2017 (see primer positions on the scheme above histograms). The copy number in *cn*^{1} *bw*^{1}*/SD-Mad* was set to 1000 based on Khost *et al.* (2017). (B) The cytological phenotype of *RAL-380/SD-Mad* (top right panels), *RAL-309/SD-Mad* (bottom left panels), and *RAL-313/SD-Mad* (bottom right panels) testes carrying the *protB-GFP* transgene and stained with an anti-dsDNA antibody (dsDNA-Ab; red), phalloidin (not shown for clarity) and DAPI (blue). *RAL-380/SD-Mad* which carry ca. 2500-2700 copies present a

phenotype similar to *Gla/SD5* males. About half of the nuclei incorporate less protamines and are abnormally compacted as revealed by the bright anti-dsDNA staining (pre-IC and IC cysts). These nuclei are eliminated during individualization (IC and post-IC) and seminal vesicles contain almost no abnormal anti-dsDNA positive nuclei. In *RAL-309/SD-Mad* (ca. 1300 *Rsp* copies), although protamine incorporation is also delayed in half of nuclei (pre-IC), many anti-dsDNA positive nuclei are detected in the bundle of spermatid after individualization (arrow). These abnormally condensed nuclei are detected in seminal vesicles. In *RAL-313/SD-Mad* males (ca. 1000 copies), protamine incorporation appears less disturbed but many anti-dsDNA positive nuclei are detected during individualization, in the bundle of spermatid nuclei after individualization (arrow) and in seminal vesicles. Scale bar: 10µm.

Figure 7: *SD* male cytological phenotypes are modified by a suppressor on the X chromosome

(A) Confocal images of seminal vesicles stained with an anti-dsDNA antibody (dsDNA-Ab; red), phalloidin (white) and DAPI (blue) from *RAL-380/SD-Mad*, *RAL-309/SD-Mad* , and *RAL-313/SD-Mad* males carrying the *protB-GFP* transgene with the X chromosome from the w^{1118}*; SD-Mad/CyO; protB-GFP* lines, which does not carry a suppressor (left panels) or from the *RAL* strains which carries *Su(SD)X* (right panels). Scale bars: 50µm for large views of the seminal vesicles and 10µm for zoom-ins (B) A box plot showing a quantification of the percentage of anti-dsDNA positive sperm nuclei in seminal vesicles of the genotypes shown in (A). Whiskers show minimum and maximum values, boxes show the middle 50% of the values and horizontal lines represent medians. For each genotype, five seminal vesicles from five different males were analyzed. Wilcoxon test, ** p-value<0.01.

Figure 8: A model for spermatid elimination in SD males

In control males carrying a large *Rsp* satDNA block, *Rsp* heterochromatin organization allows the histone-to-protamine transition to occur normally. Spermatids thus individualize and are released in the seminal vesicle. In *SD* males carrying a SD^+ Rsp^s chromosome with ca.1000 copies, *Rsp* satDNA chromatin state slightly perturbs SNBP incorporation. In some SD^+ Rsp^s nuclei, chromatin compaction defects are too important and trigger differentiation arrest. These nuclei are eliminated during individualization and end up in the waste bag. In some other SD^+ Rsp^s nuclei, nuclear compaction defects are weaker and spermiogenesis progress normally. In this case, abnormally compacted needle-shaped SD^+ Rsp^s sperm nuclei are released in the seminal vesicle. In *SD* males carrying a SD^+ Rsp^{ss} chromosome (> 2,000 copies), *Rsp* satDNA chromatin impairs SNBP incorporation and nuclear compaction defects trigger the elimination of SD^+ Rsp^{ss}during individualization.

Figure S1: Spermatogenesis in *SD* males

(A) Confocal images of fly whole-mount testes from a control *SD5/CyO; protB-GFP* and a distorter *cn*^{1} *bw*^{1}*/SD-Mad; protB-GFP* male stained with DAPI (blue), and antibodies against histones (red) and Vasa (white). Scale bar: 100µm in large views and 20µm in magnified squares. (B) Cysts of 64 spermatid nuclei after individualization stained for DNA (DAPI) and Protamine-GFP (green). Scale bar: 10µm.

Figure S2: An anti-dsDNA antibody to probe for chromatin compaction.

Confocal images of a whole-mount testis stained with DAPI (blue), F-actin (white) and the anti-dsDNA antibody (dsDNA-Ab; red). Top panels show the nucleus of a somatic cell next to a sperm cell nucleus (arrow). While the somatic nucleus is brightly stained with the anti-dsDNA antibody, the sperm nucleus is impermeant to it. DAPI staining intensity is proportional to DNA compaction and brightly stains highly compacted DNA such as heterochromatin (yellow arrow) in somatic nuclei. On the opposite, the anti-dsDNA staining is inversely proportional to chromatin compaction and is weak in heterochromatic regions. Bottom panels show three cysts of 64 spermatid nuclei at different stages. The two cysts on top contain elongating spermatid nuclei before individualization. These nuclei are stained with the anti-dsDNA antibody. The bottom cyst contains nuclei which have been invested by individualization actin cones. At this stage, nuclei are negative for the anti-dsDNA staining because of the high compaction of chromatin. Asterisk indicates a somatic nucleus. Scale bar: 10µm.

Figure S3: Seminal vesicles contents in *Gla/CyO* control males

(A) Confocal images of a whole-mount seminal vesicle from a *Gla/CyO; protB-GFP* control male stained with an anti-dsDNA antibody (dsDNA-Ab; red), DAPI (blue) and phalloidin (white). A wide view of the seminal vesicle is shown on the left panel (scale bar: 50µm). The dashed white square corresponds to a magnified region shown on right panels (scale bar: 10µm). Almost all sperm nuclei are negative for the anti-dsDNA antibody and are thus properly compacted. (B) DNA-FISH performed on seminal vesicle contents with a *Rsp* probe (green) and a probe for the *359 bp* satDNA (red) on the X chromosome as a control (scale bar: 10µm). Sperm nuclei appear larger in all panels because they have been treated with DTT to facilitate probe penetration.

Figure S4: The histone-to-protamine transition in *cn^1 bw^1/SD5* and *Gla/SD-Mad* distorter males

Confocal images of whole-mount testes from *Gla/SD-Mad; protB-GFP* and *cn^1 bw^1/SD5; protB-GFP* males stained with an anti-dsDNA antibody (dsDNA-Ab; red), DAPI (blue) and phalloidin (F-actin, white). In *Gla/SD-Mad*, many abnormally-shaped nuclei that are weakly stained with ProtB-GFP and brightly stained with the anti-dsDNA antibody are visible in pre-IC, IC and post-IC cysts. In *cn^1 bw^1/SD5* testes, abnormally-shaped anti-dsDNA positive nuclei are less frequent. Bundles of post-IC spermatid contain needle-shaped anti-dsDNA positive nuclei. Scale bar: 10µm.

Figure S5: DNA-FISH on spermatid nuclei

(A) DNA-FISH on squashed testes from *cn^1 bw^1/CyO, Gla/CyO, RAL-313* and *RAL-309 and RAL-380* males performed with a *Rsp* (green) and a *359 bp* (red) probe. Scale bar: 10µm (B) Box plot showing the ratio of *Rsp* signal area over nuclear area expressed as a percentage. For each genotype, the number of isolated nuclei analyzed is indicated. The area of *Rsp* signals is larger in *Gla* spermatids compared to in *cn^1 bw^1* nuclei, in agreement with molecular quantification. Area of *Rsp*

satDNA in *RAL* strains are also proportional to copy numbers determined by qPCR. Wilcoxon test, non-significant (ns) p-value>0.05, * p-value <0.05, ** p-value<0.01, ***p-value<0.001.

Figure S6: Su(SD)X modifies the histone-to-protamine transition and individualization phenotypes of *RAL-380/SD-Mad* males.

Confocal images of *RAL-380/SD-Mad; protB-GFP* testes carrying the X chromosome from the *RAL-380* strain with *Su(SD)X-380* suppressor (right panels) or the w^{1118} chromosome (left panels). Protamine incorporation and individualization appear less disturbed in presence of *Su(SD)X-380*. Bundles of individualized spermatid nuclei (post-IC) are less disturbed but include many needle-shaped nuclei positively stained with the anti-dsDNA antibody. Scale bar: 10µm

Figure S7: Cross schemes to obtain the different genotypes of distorter and control males

Figure S8: Cross scheme to obtain the *Cy SD-Mad* chromosome

Genotype of fathers	*k* value	n	X chromosome
SD-Mad/CyO; protB-GFP	0.443 ±0.074	1471	w^{1118} (from *Gla/CyO*)
SD5/CyO; protB-GFP	0.338 ±0.076	1483	w^{1118} (from *Gla/CyO*)
cn^1 bw^1/ CyO; *protB-GFP*	0.526 ±0.044	1403	y^1 (from cn^1 bw^1)
Gla/ CyO; protB-GFP	0.505 ±0.051	2530	w^{1118} (from *Gla/CyO*)
cn^1 bw^1/*SD-Mad; protB-GFP*	0.998 ±0.005	705	y^1 (from cn^1 bw^1)
Gla/SD5; protB-GFP	1 ±0.00	938	w^{1118} (from *Gla/CyO*)
Gla /SD-Mad; protB-GFP	0.999 ±0.004	1214	w^{1118} (from *Gla/CyO*)
cn^1 bw^1/*SD5; protB-GFP*	0.999 ±0.003	1012	y^1 (from cn^1 bw^1)
RAL-313/SD-Mad, Cy	0.975 ±0.013	2579	X from *SD-Mad, Cy*
RAL-313/ SD-Mad, Cy	0.757 ±0.071	1622	X from *RAL-313*
RAL-309/ SD-Mad, Cy	0.956 ±0.058	2270	X from *SD-Mad, Cy*
RAL-309/ SD-Mad, Cy	0.927 ±0.067	2228	X from *RAL-309*
RAL-380/SD-Mad, Cy	0.997 ±0.004	2598	X from *SD-Mad, Cy*
RAL-380/SD-Mad, Cy	0.941 ±0.031	2185	X from *RAL-380*

Table 1: Segregation distortion levels.
Unweighted means of *k* values ±standard deviation. n represents the number of flies in the offspring. For all male genotypes, *k* value is the ratio of offspring carrying the SD chromosome over the total number of flies except for or cn^1 bw^1/ CyO; *protB-GFP* and *Gla/ CyO; protB-GFP* males. For these two genotypes, the *k* value represents the ratio of the offspring carrying the *CyO* chromosome over the total number of flies. The X chromosome carried by tested males is also indicated. The X chromosomes of the *RAL-380, RAL-313* and *RAL-309* strains carry a suppressor. A description of the crosses to obtain distorter and control genotypes are provided on Figure S7.

Figure 1

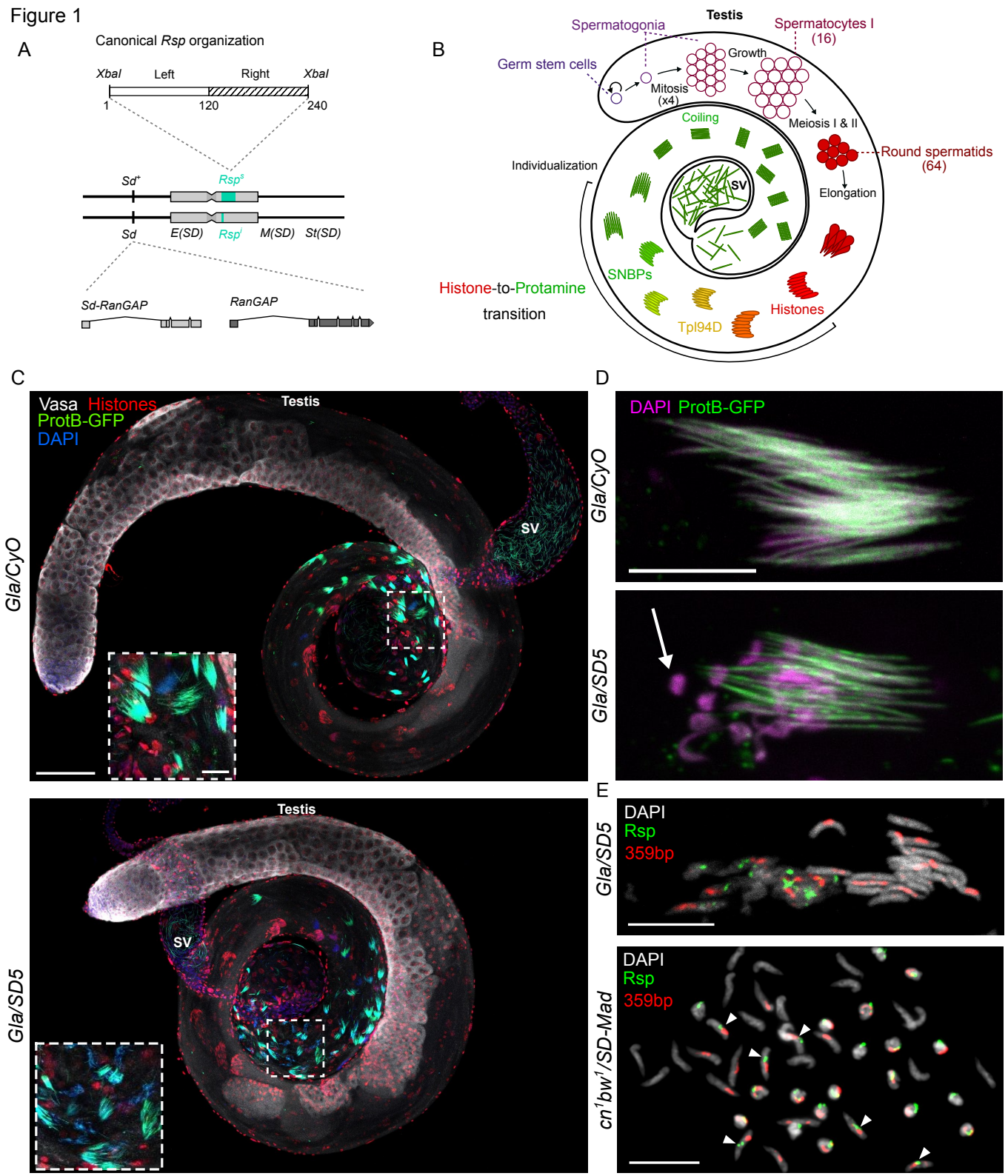
A
Canonical Rsp organization
XbaI
Left
Right
XbaI
1
120
240
Sd+
Rsps
Sd
E(SD)
Rspi
M(SD)
St(SD)
Sd-RanGAP
RanGAP
B
Testis
Spermatogonia
Spermatocytes I
(16)
Germ stem cells
Growth
Mitosis
(x4)
Meiosis I & II
Coiling
Round spermatids
(64)
Individualization
SV
Elongation
SNBPs
Histone-to-Protamine
transition
Histones
Tpl94D
C
Vasa Histones
ProtB-GFP
DAPI
Testis
SV
Gla/CyO
Testis
SV
Gla/SD5
D
DAPI ProtB-GFP
Gla/CyO
Gla/SD5
E
DAPI
Rsp
359bp
Gla/SD5
DAPI
Rsp
359bp
cn1bw1/SD-Mad

Figure 2

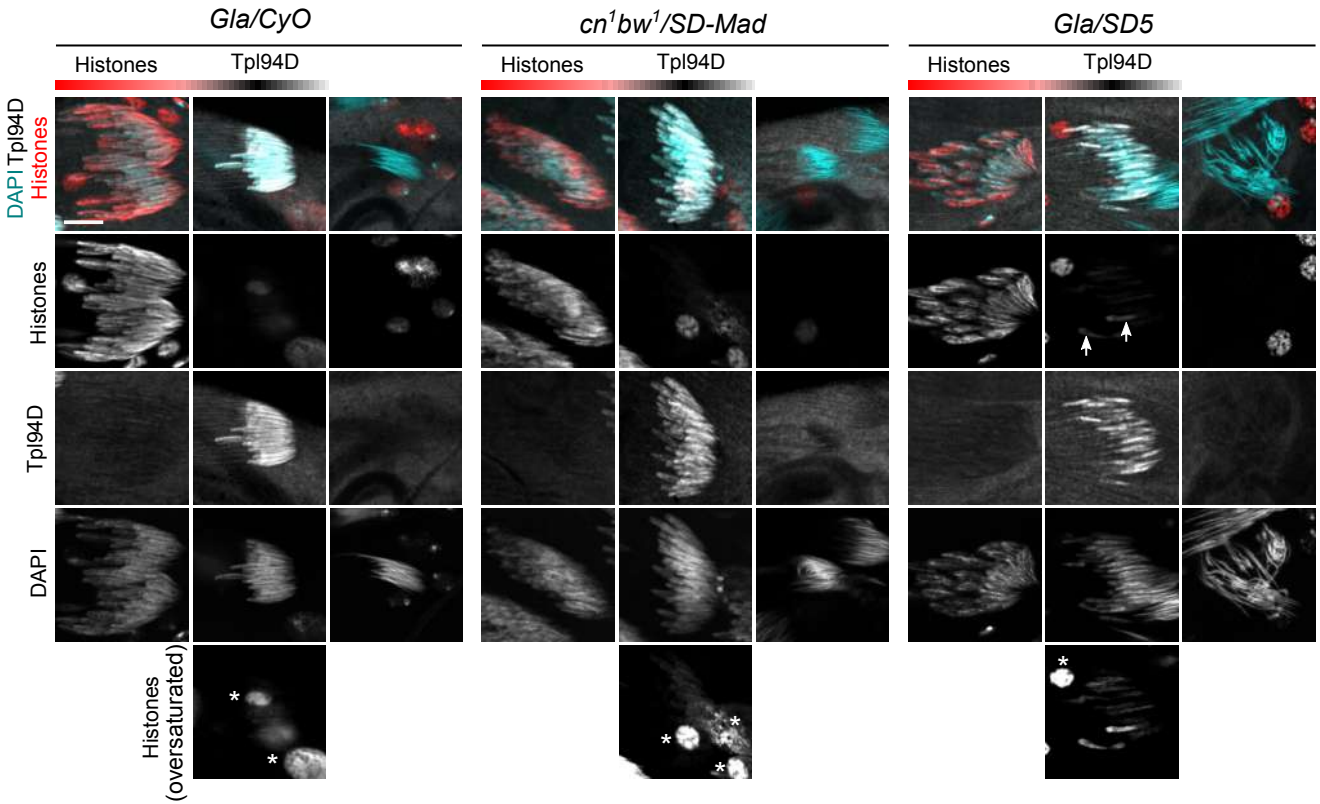
Gla/CyO
cn1bw1/SD-Mad
Gla/SD5
Histones
Tpl94D
DAPI Tpl94D
Histones
Histones
Tpl94D
DAPI
Histones (oversaturated)

Figure 3

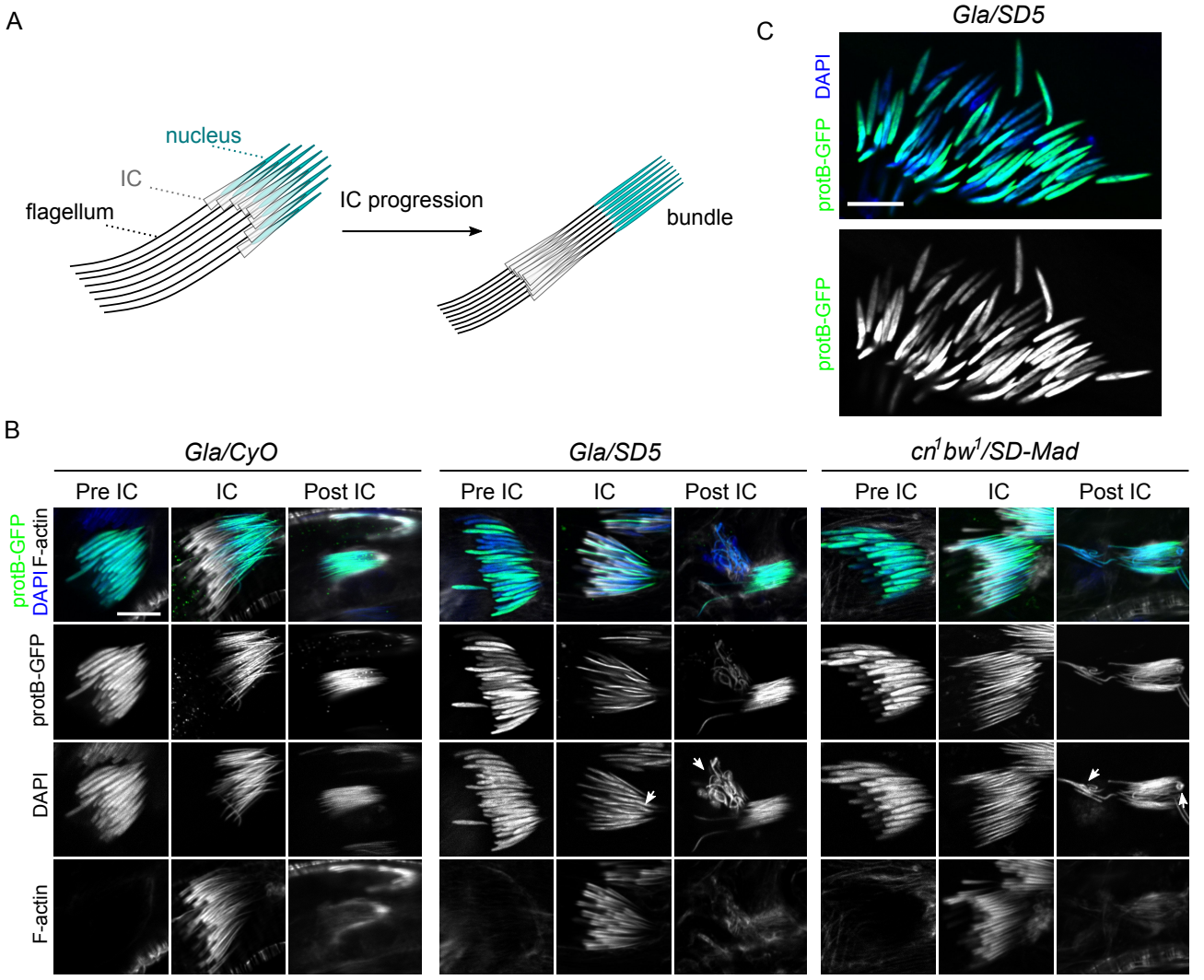
A
nucleus
IC
flagellum
IC progression
bundle
C
Gla/SD5
DAPI
protB-GFP
protB-GFP
B
Gla/CyO
Gla/SD5
cn1 bw1/SD-Mad
Pre IC
IC
Post IC
protB-GFP
DAPI F-actin
protB-GFP
DAPI
F-actin

Figure 4

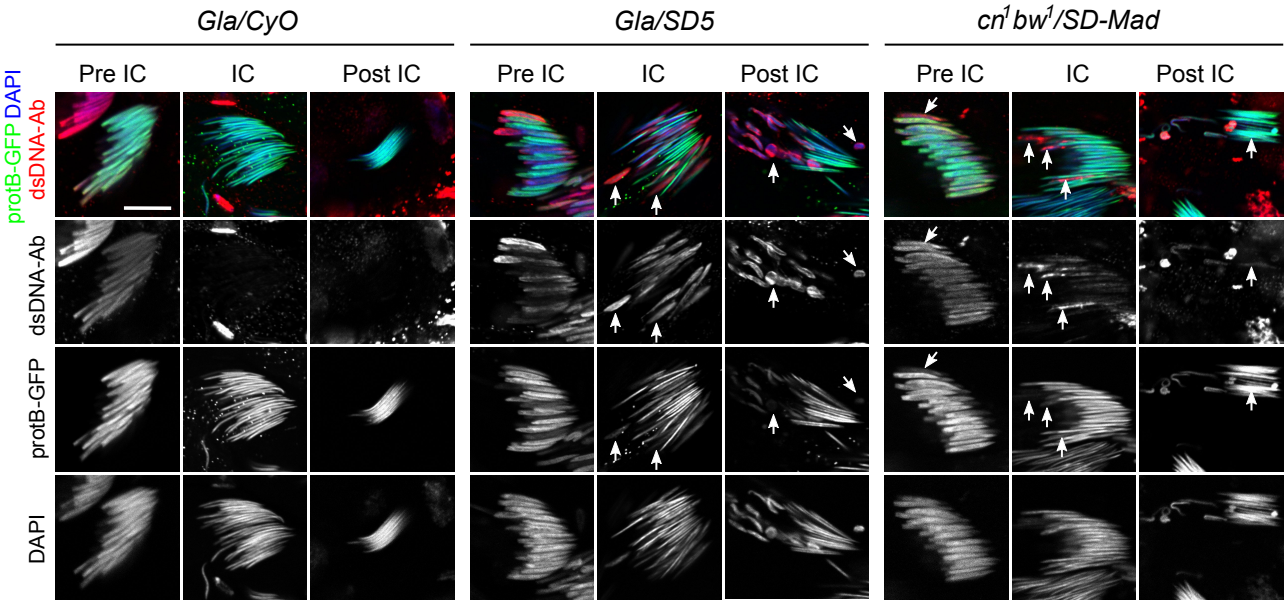
Gla/CyO
Gla/SD5
cn1 bw1/SD-Mad
Pre IC
IC
Post IC
Pre IC
IC
Post IC
Pre IC
IC
Post IC
protB-GFP DAPI
dsDNA-Ab
dsDNA-Ab
protB-GFP
DAPI

Figure 5

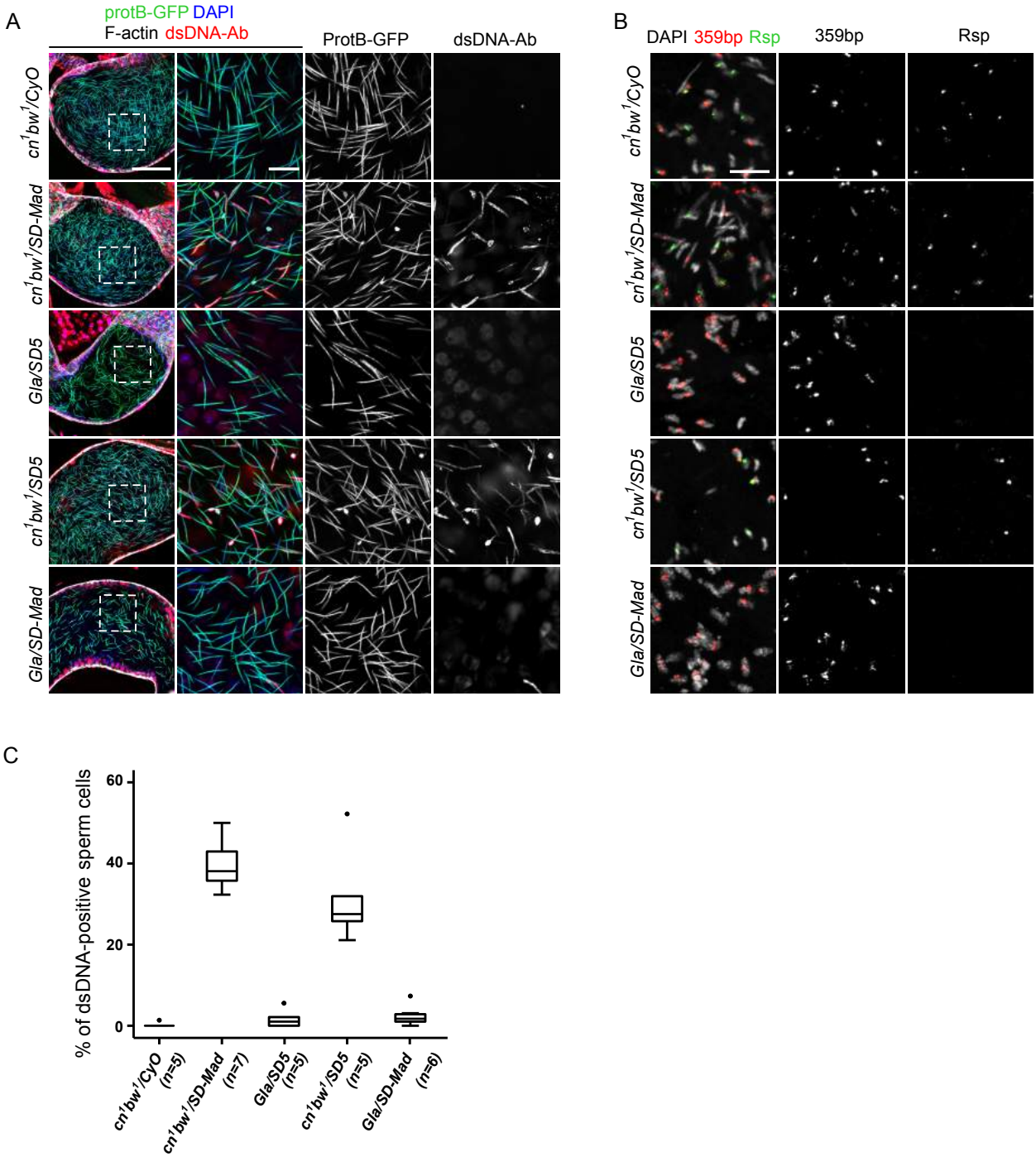
A
protB-GFP DAPI
F-actin dsDNA-Ab
ProtB-GFP
dsDNA-Ab
cn1bw1/CyO
cn1bw1/SD-Mad
Gla/SD5
cn1bw1/SD5
Gla/SD-Mad
B
DAPI 359bp Rsp
359bp
Rsp
cn1bw1/CyO
cn1bw1/SD-Mad
Gla/SD5
cn1bw1/SD5
Gla/SD-Mad
C
% of dsDNA-positive sperm cells
60
40
20
0
cn1bw1/CyO (n=5)
cn1bw1/SD-Mad (n=7)
Gla/SD5 (n=5)
cn1bw1/SD5 (n=5)
Gla/SD-Mad (n=6)

Figure 6

A

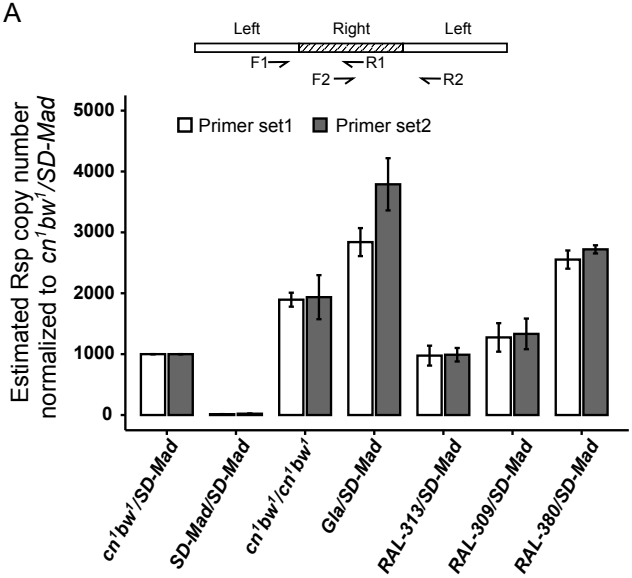
Left
Right
Left
F1
R1
F2
R2
Primer set1
Primer set2
Estimated Rsp copy number normalized to cn1bw1/SD-Mad
5000
4000
3000
2000
1000
0
cn1bw1/SD-Mad
SD-Mad/SD-Mad
cn1bw1/cn1bw1
Gla/SD-Mad
RAL-313/SD-Mad
RAL-309/SD-Mad
RAL-380/SD-Mad

B

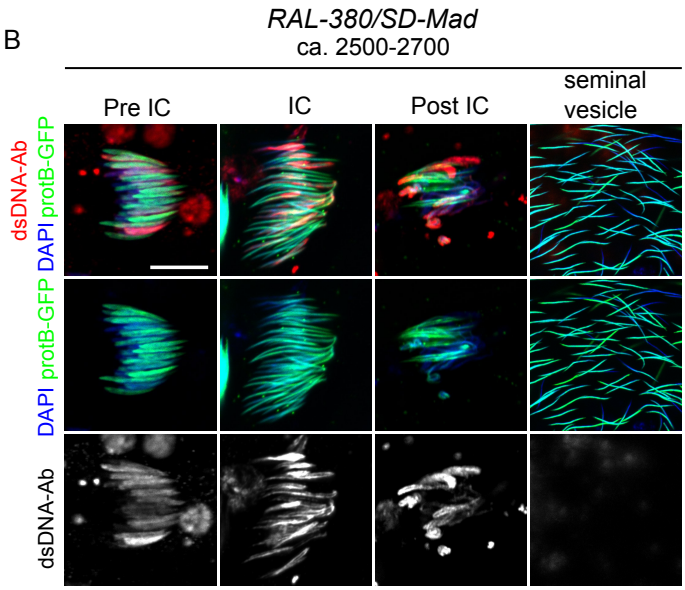
RAL-380/SD-Mad
ca. 2500-2700
Pre IC
IC
Post IC
seminal vesicle
dsDNA-Ab
DAPI protB-GFP
DAPI protB-GFP
dsDNA-Ab

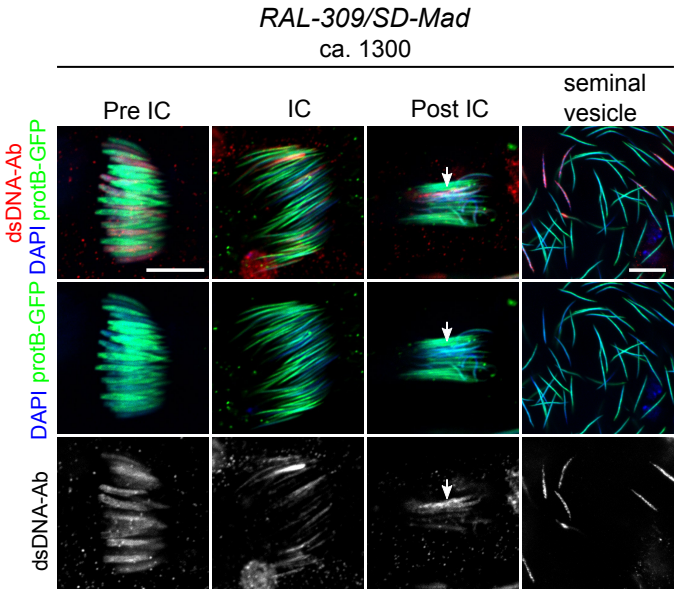
RAL-309/SD-Mad
ca. 1300
Pre IC
IC
Post IC
seminal vesicle
dsDNA-Ab
DAPI protB-GFP
DAPI protB-GFP
dsDNA-Ab

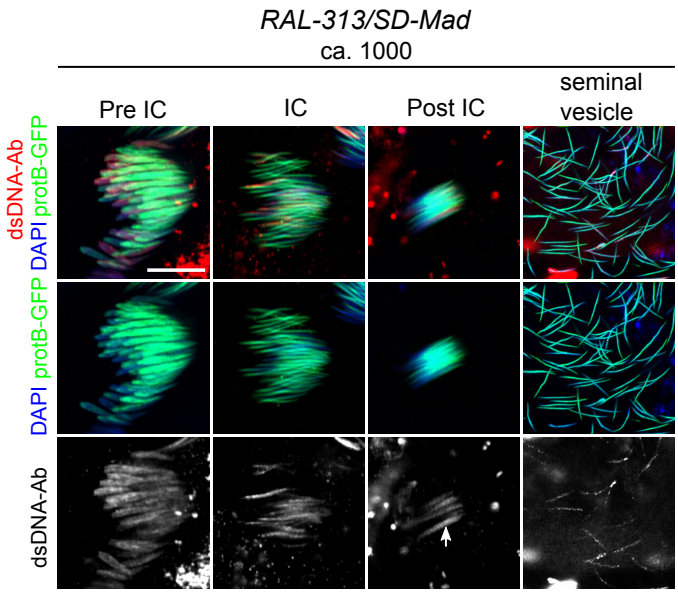
RAL-313/SD-Mad
ca. 1000
Pre IC
IC
Post IC
seminal vesicle
dsDNA-Ab
DAPI protB-GFP
DAPI protB-GFP
dsDNA-Ab

Figure 7

A

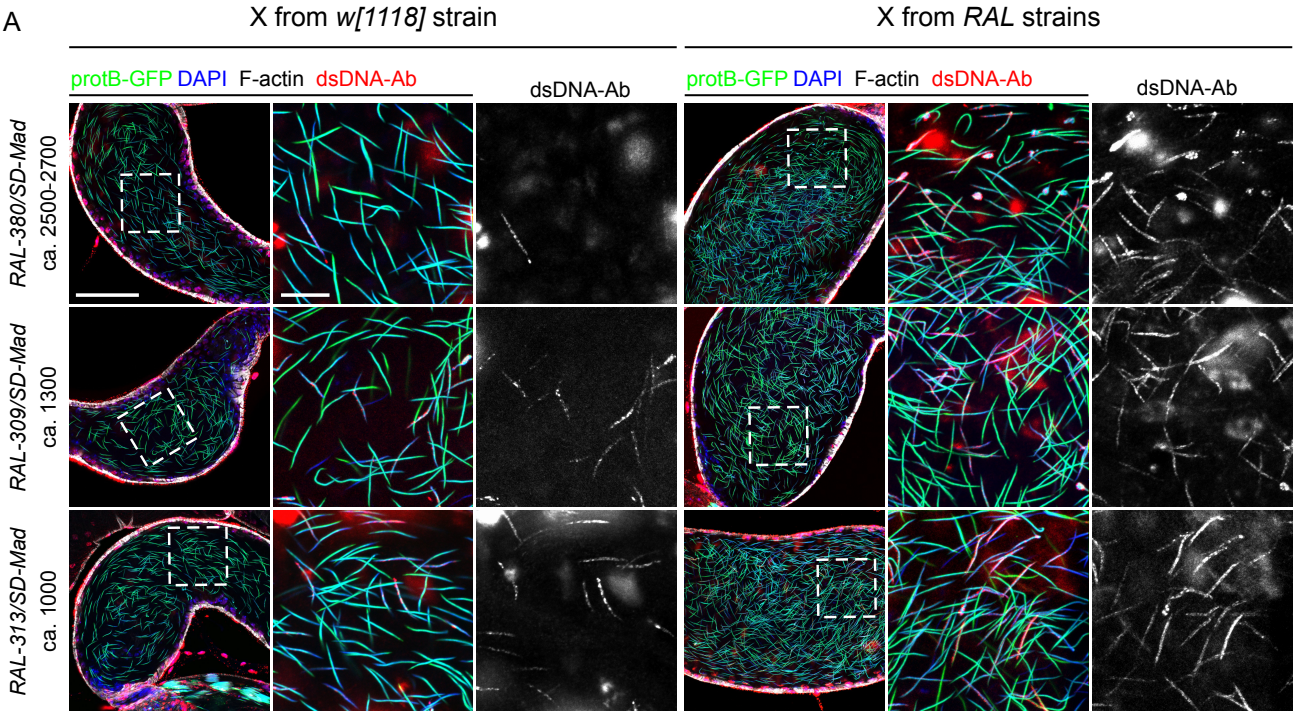
X from w[1118] strain
X from RAL strains
protB-GFP DAPI F-actin dsDNA-Ab
dsDNA-Ab
protB-GFP DAPI F-actin dsDNA-Ab
dsDNA-Ab
RAL-380/SD-Mad
ca. 2500-2700
RAL-309/SD-Mad
ca. 1300
RAL-313/SD-Mad
ca. 1000

B

% of dsDNA-positive sperm cells
60
40
20
0
**
**
**
RAL-380/SD-Mad
RAL-309/SD-Mad
RAL-313/SD-Mad
X from w[1118] strain
X from RAL strains

Figure 8

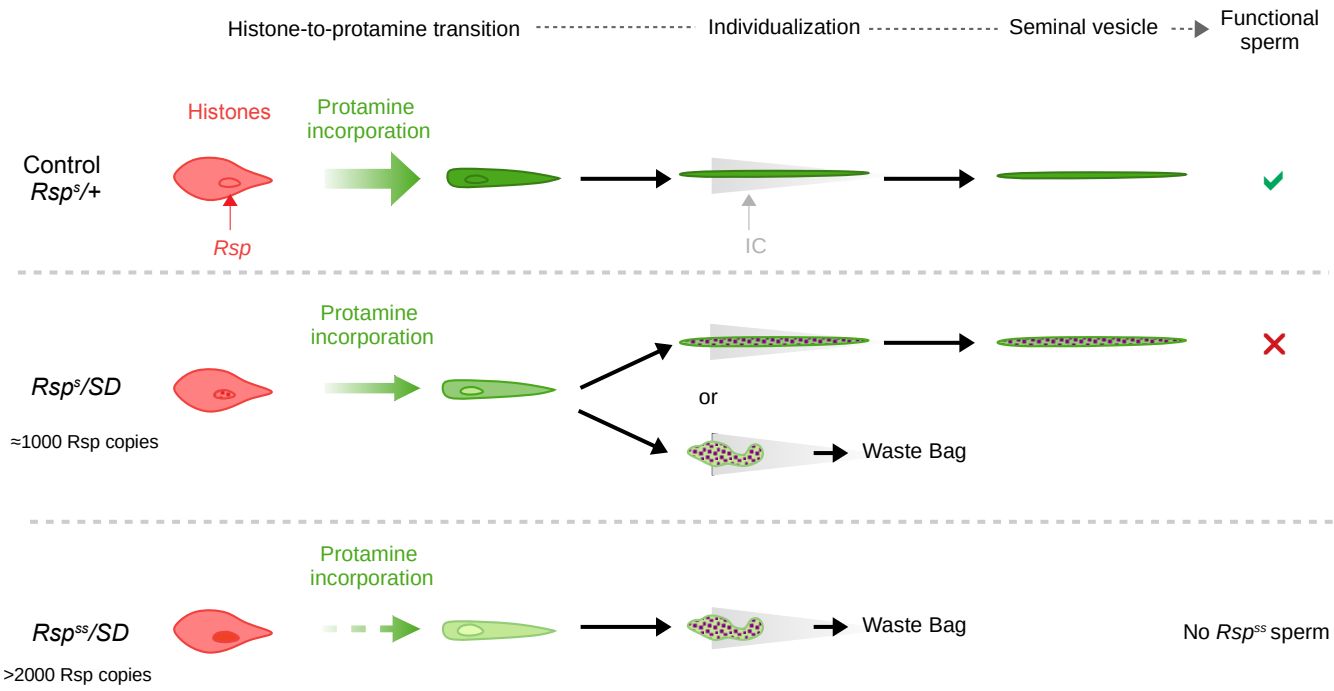
Histone-to-protamine transition
Individualization
Seminal vesicle
Functional sperm
Histones
Protamine incorporation
Control
Rsp^s/+
Rsp
IC
Protamine incorporation
Rsp^s/SD
≈1000 Rsp copies
or
Waste Bag
Protamine incorporation
Rsp^ss/SD
>2000 Rsp copies
Waste Bag
No Rsp^ss sperm

Figure S1

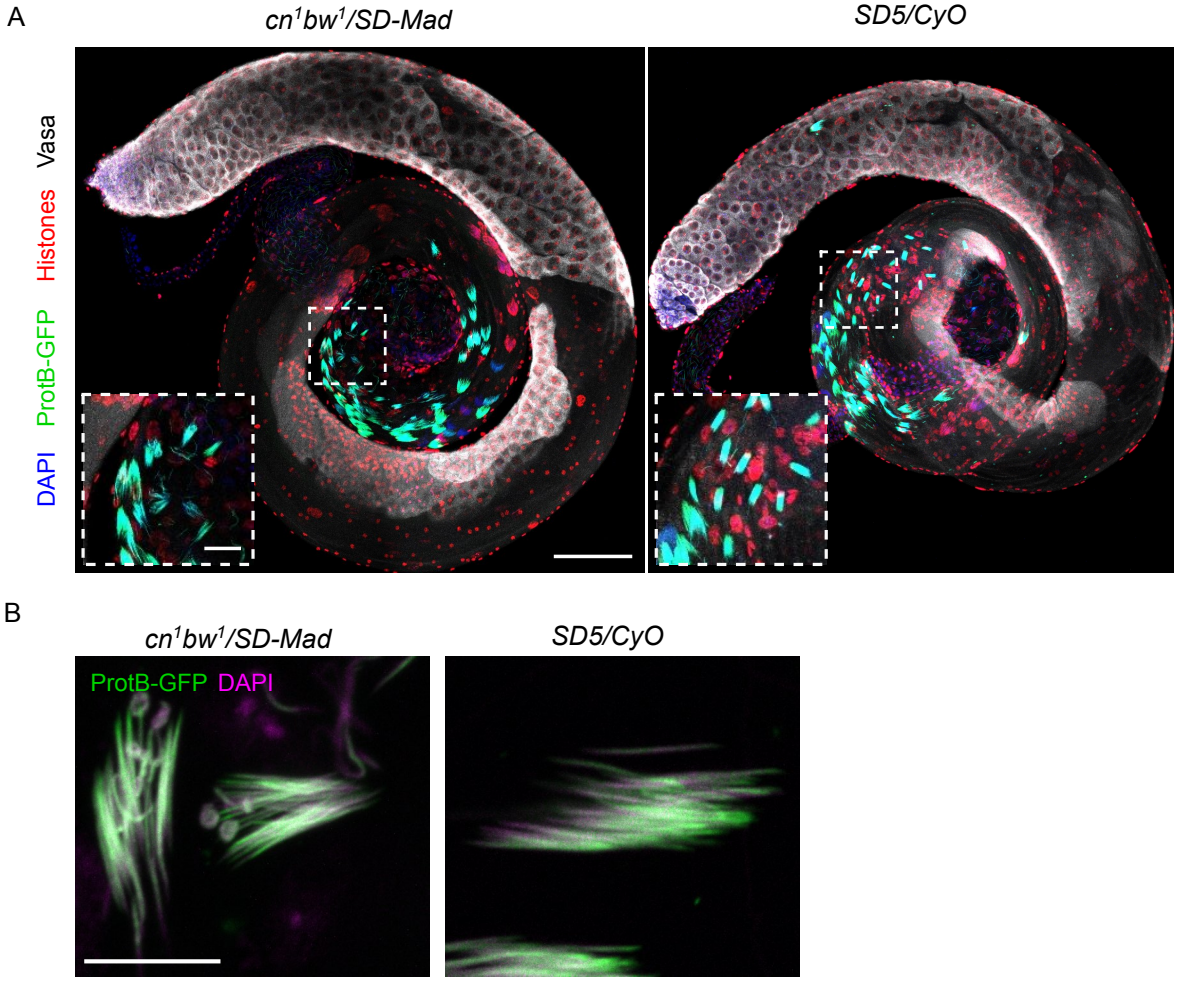
A
cn1bw1/SD-Mad
SD5/CyO
Vasa
Histones
ProtB-GFP
DAPI
B
cn1bw1/SD-Mad
SD5/CyO
ProtB-GFP DAPI

Figure S2

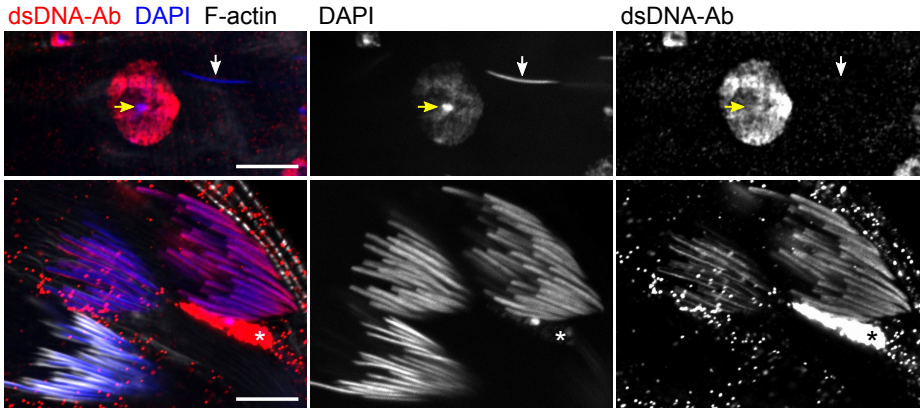

Figure S3

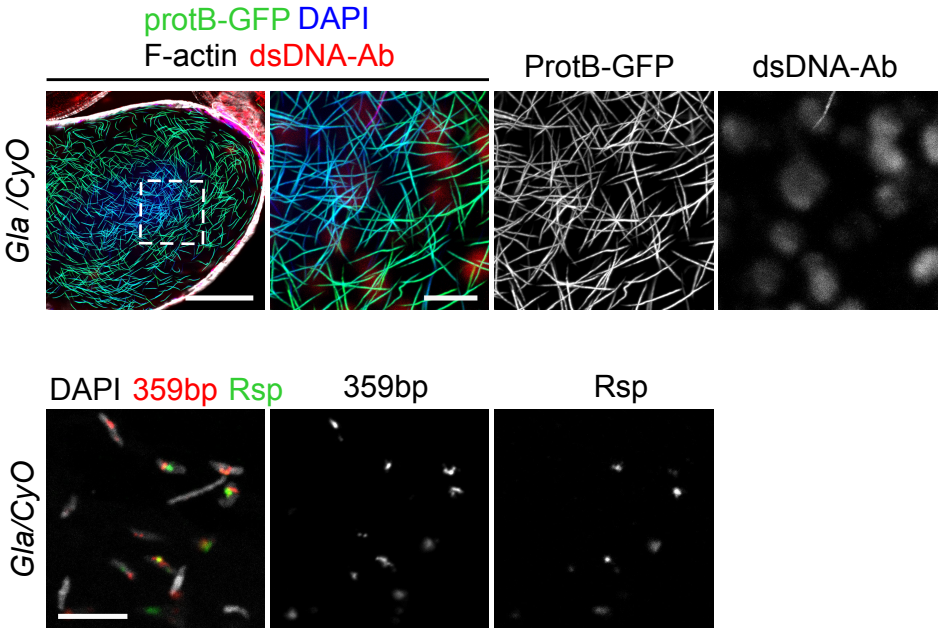
protB-GFP DAPI
F-actin dsDNA-Ab
ProtB-GFP
dsDNA-Ab
Gla /CyO
DAPI 359bp Rsp
359bp
Rsp
Gla/CyO

Figure S4

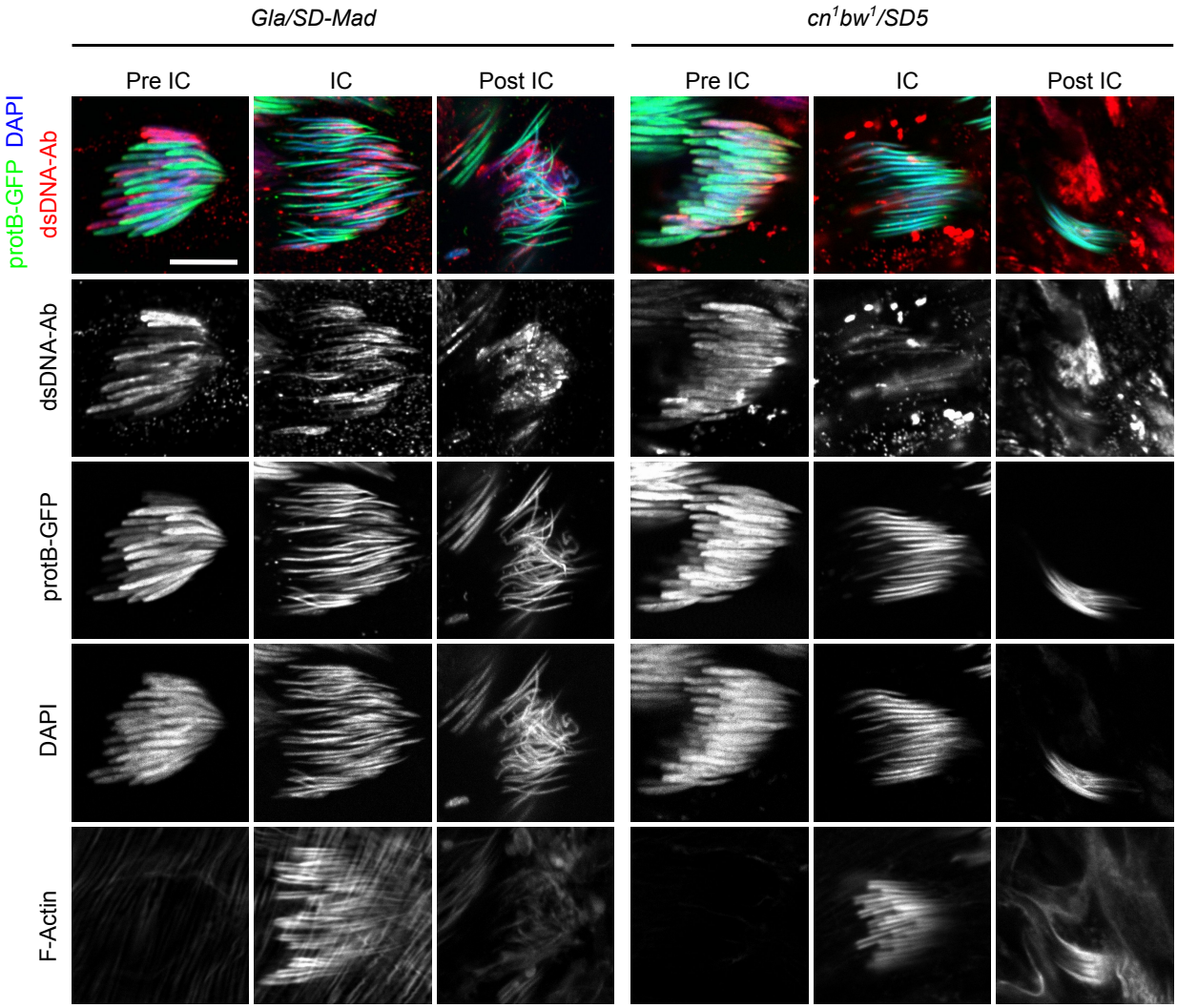
Gla/SD-Mad
cn1bw1/SD5
Pre IC
IC
Post IC
Pre IC
IC
Post IC
protB-GFP DAPI
dsDNA-Ab
dsDNA-Ab
protB-GFP
DAPI
F-Actin

Figure S5

A

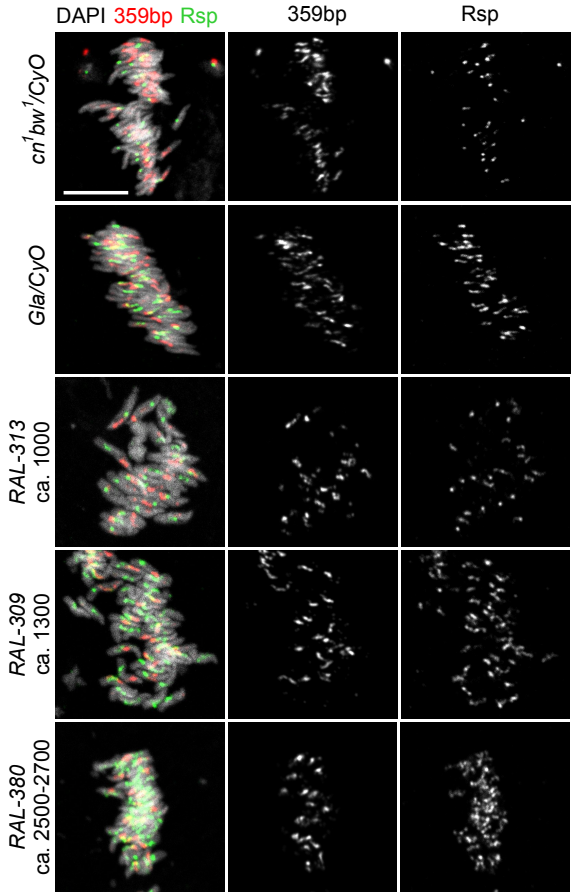
DAPI 359bp Rsp
359bp
Rsp
cn1bw1/CyO
Gla/CyO
RAL-313 ca. 1000
RAL-309 ca. 1300
RAL-380 ca. 2500-2700

B

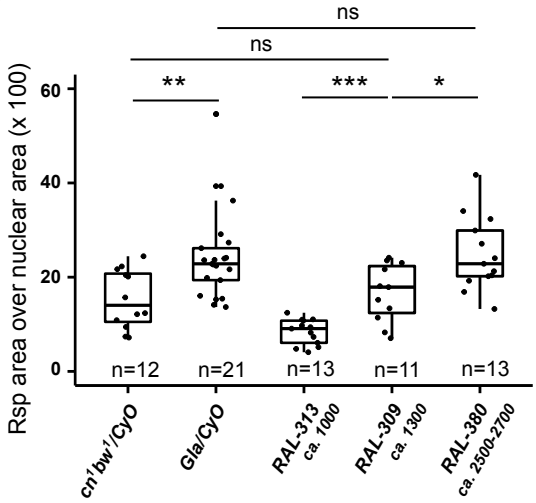
ns
ns
**
***
*
Rsp area over nuclear area (x 100)
60
40
20
0
n=12
n=21
n=13
n=11
n=13
cn1bw1/CyO
Gla/CyO
RAL-313 ca. 1000
RAL-309 ca. 1300
RAL-380 ca. 2500-2700

Figure S6

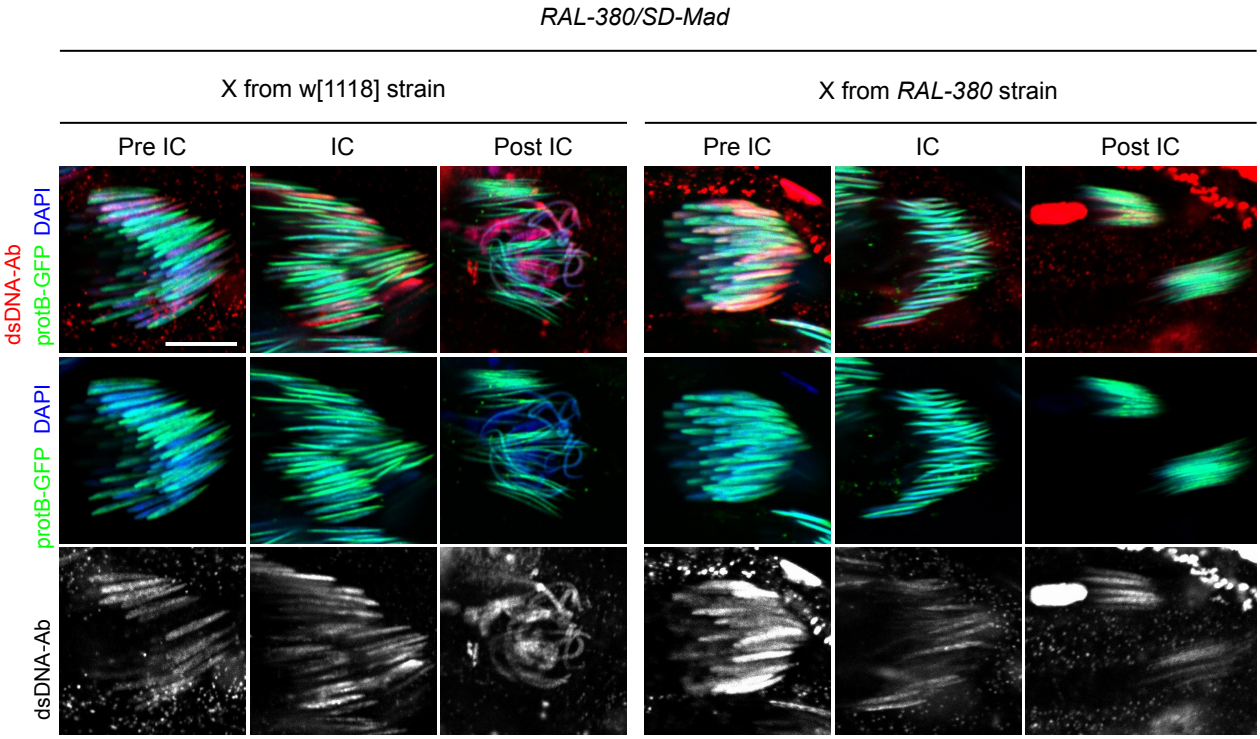
RAL-380/SD-Mad
X from w[1118] strain
X from RAL-380 strain
Pre IC
IC
Post IC
Pre IC
IC
Post IC
dsDNA-Ab
protB-GFP
DAPI
protB-GFP
DAPI
dsDNA-Ab

Figure S7

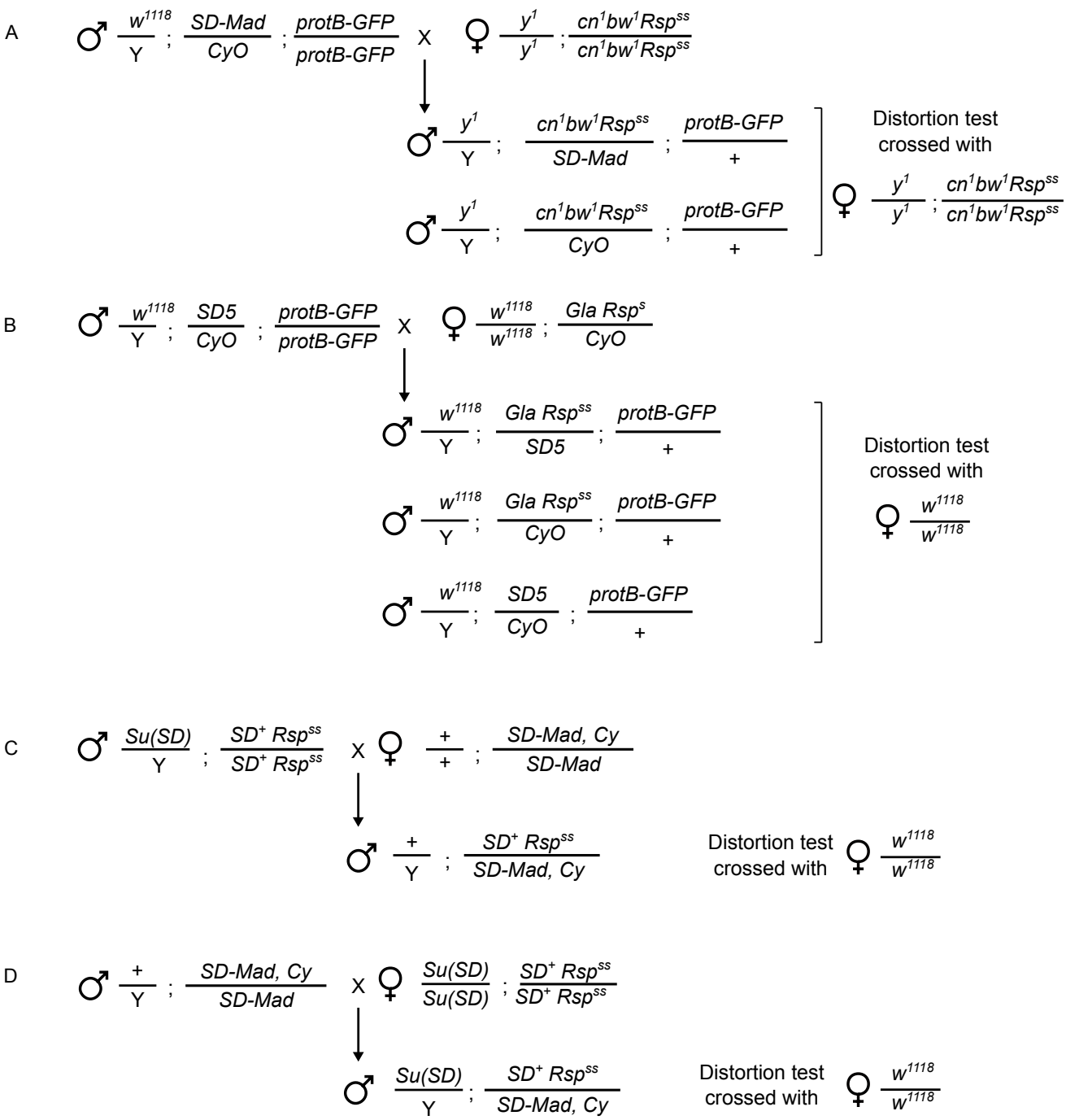
A
♂ w1118/Y ; SD-Mad/CyO ; protB-GFP/protB-GFP X ♀ y1/y1 ; cn1bw1Rspss/cn1bw1Rspss
♂ y1/Y ; cn1bw1Rspss/SD-Mad ; protB-GFP/+
♂ y1/Y ; cn1bw1Rspss/CyO ; protB-GFP/+
Distortion test crossed with
♀ y1/y1 ; cn1bw1Rspss/cn1bw1Rspss
B
♂ w1118/Y ; SD5/CyO ; protB-GFP/protB-GFP X ♀ w1118/w1118 ; Gla Rsps/CyO
♂ w1118/Y ; Gla Rspss/SD5 ; protB-GFP/+
♂ w1118/Y ; Gla Rspss/CyO ; protB-GFP/+
♂ w1118/Y ; SD5/CyO ; protB-GFP/+
Distortion test crossed with
♀ w1118/w1118
C
♂ Su(SD)/Y ; SD+ Rspss/SD+ Rspss X ♀ +/+ ; SD-Mad, Cy/SD-Mad
♂ +/Y ; SD+ Rspss/SD-Mad, Cy
Distortion test crossed with ♀ w1118/w1118
D
♂ +/Y ; SD-Mad, Cy/SD-Mad X ♀ Su(SD)/Su(SD) ; SD+ Rspss/SD+ Rspss
♂ Su(SD)/Y ; SD+ Rspss/SD-Mad, Cy
Distortion test crossed with ♀ w1118/w1118

Figure S8

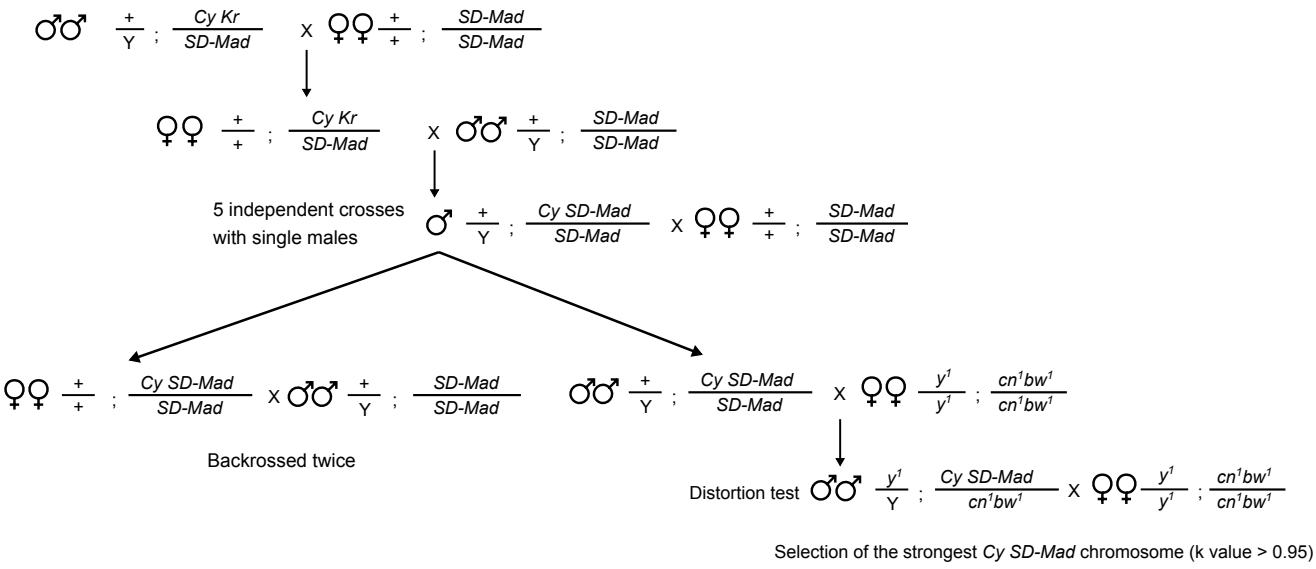
♂♂ + / Y ; Cy Kr / SD-Mad x ♀♀ + / + ; SD-Mad / SD-Mad
♀♀ + / + ; Cy Kr / SD-Mad x ♂♂ + / Y ; SD-Mad / SD-Mad
5 independent crosses
with single males
♂ + / Y ; Cy SD-Mad / SD-Mad x ♀♀ + / + ; SD-Mad / SD-Mad
♀♀ + / + ; Cy SD-Mad / SD-Mad x ♂♂ + / Y ; SD-Mad / SD-Mad
Backrossed twice
♂♂ + / Y ; Cy SD-Mad / SD-Mad x ♀♀ y1 / y1 ; cn1bw1 / cn1bw1
Distortion test ♂♂ y1 / Y ; Cy SD-Mad / cn1bw1 x ♀♀ y1 / y1 ; cn1bw1 / cn1bw1
Selection of the strongest Cy SD-Mad chromosome (k value > 0.95)